3-2022

Intercomparison of Four Microphysics Schemes in Simulating Persistent Arctic Mixed-Phase Stratocumulus Clouds

Zachary A. Cleveland

Intercomparison of Four Microphysics Schemes in Simulating Persistent Arctic Mixed-Phase Stratocumulus Clouds

THESIS

Zachary A. Cleveland, Captain, U.S. Air Force

AFIT-ENP-MS-22-M-084

DEPARTMENT OF THE AIR FORCE
AIR UNIVERSITY

AIR FORCE INSTITUTE OF TECHNOLOGY

Wright-Patterson Air Force Base, Ohio

AFIT-ENP-MS-22-M-084

INTERCOMPARISON OF FOUR MICROPHYSICS SCHEMES IN SIMULATING PERSISTENT ARCTIC MIXED-PHASE STRATOCUMULUS CLOUDS

THESIS

Presented to the Faculty

Department of Engineering Physics

Graduate School of Engineering and Management

Air Force Institute of Technology

Air University

Air Education and Training Command

in Partial Fulfillment of the Requirements for the

Degree of Master of Science in Atmospheric Science

Zachary A. Cleveland, B.S.

Captain, U.S. Air Force

March 2022

AFIT-ENP-MS-22-M-084

INTERCOMPARISON OF FOUR MICROPHYSICS SCHEMES IN SIMULATING PERSISTENT ARCTIC MIXED-PHASE STRATOCUMULUS CLOUDS

THESIS

Zachary A. Cleveland, B.S.
Captain, U.S. Air Force

Committee Membership:

Lt Col Kyle E. Fitch, Ph.D.
Chair

Maj Peter A. Saunders, Ph.D.
Reader

Ann M. Fridlind, Ph.D.
Reader

Lt Col H. Rose Tseng, Ph.D.
Reader

Abstract

Persistent Arctic mixed-phase stratocumulus clouds (AMPS) are important to the surface radiation budget of the Arctic and their presence produces warming within the boundary layer and at the surface. Inaccurately forecasting AMPS can lead to large, erroneous temperature forecasts and consequently, further model forecast errors. A Large Eddy Simulation of a case study of a persistent AMPS cloud was conducted using the Advanced Research Weather Research and Forecasting (WRF-ARW) model. The case examined occurred near Oliktok Point, AK between 26 and 27 April, 2017. The produced cloud pattern and properties of four different microphysics schemes – P3, Thompson, Morrison, and WSM6 – are compared to observations. Results show that the Thompson scheme was able to best simulate observed conditions as a result of fewer aerosols acting as ice nucleating particles, which allowed the production of more liquid water within the cloud layer. Thompson was the only parameterization scheme to produce significant cloud liquid water, which resulted in additional cloud top radiative cooling, continued coupling with the surface, and sustainment of the cloud layer. The lack of cloud liquid water produced in the other three schemes resulted in the early dissipation of their cloud layers and, consequently, stronger surface cooling, which led to production of a surface-based inversion and a decoupling of the cloud layer. Due to the Thompson scheme's more accurate representation of the cloud structure, it also captured surface and cloud top temperatures which aligned more closely to observations. It's clear that the treatment of aerosols to act as ice nucleating particles or cloud condensation nuclei is important to AMPS and future studies should examine the magnitude to which aerosol concentrations within numerical models influence AMPS development and sustainment.

Dedicated to my dogs, Spud and Petey Potato.

Acknowledgements

I would like to thank my advisor, Lieutenant Colonel (Lt Col) Kyle Fitch, for his patience and guidance. I would also like to thank the members of my committee, Major Peter Saunders, Dr. Ann Fridlind, and Lt Col Rose Tseng, for their guidance, support, and willingness to answer my questions.

This project would have been several orders of magnitude more difficult if not for Dr. McKenna Stanford, who helped me navigate all of the difficulties in setting up WRF and successfully run my simulations. Thank you, McKenna.

Lastly, I would like to thank my wife. Her tireless effort to support me in every way from taking the lead on household responsibilities to being a sounding board for me to ramble on about ideas and much, much more so that I could focus on this project means the world to me.

Zachary A. Cleveland

Table of Contents

Page

List of Figures

List of Tables

INTERCOMPARISON OF FOUR MICROPHYSICS SCHEMES IN SIMULATING PERSISTENT ARCTIC MIXED-PHASE STRATOCUMULUS CLOUDS

I. Introduction

Arctic clouds can be very different than mid-latitude clouds and are often more difficult to properly simulate in cloud and climate models (H. Morrison et al., 2012). Clouds in this region tend to be mixed-phased, containing both ice and supercooled liquid water droplets (Solomon et al., 2011), and they tend to exist within a stable atmospheric profile. The presence of these AMPS clouds can be very sensitive to various atmospheric conditions, which are discussed in more detail in chapter II. Frequently the conditions which are observed in the Arctic allow for AMPS to persist for days-to-weeks despite continuous ice precipitation (D. Wang et al., 2020; H. Morrison et al., 2012; Silber et al., 2021). Small changes to the dynamical or microphysical environment can be the difference between persistence and dissipation of AMPS clouds.

AMPS are the dominant cloud type over the Arctic for up to three-quarters of the year, with the largest frequency occurring during the spring and fall transition seasons (Intrieri et al., 2002). Typically, there are two main types of radiative state over the lower levels ($\sim$ 0.5 - 2.0 km) of the Arctic region: clear skies and opaque, cloudy conditions (H. Morrison et al., 2012). H. Morrison et al. (2012) showed that just a 5% shift in the frequency of clear skies to cloudy conditions can result in a change in the net surface longwave radiation of up to 2 $W\,m^{-2}$, and that sea ice loss over the past 30 years (relative to 2011) can be attributed to just a 1 $W\,m^{-2}$ change.

Interest in Arctic weather and the ability to forecast conditions is important for

a variety of reasons. Firstly, although population sizes tend to be smaller, there still are people who live well above the Arctic circle, and understanding future weather conditions is important for the livelihood and planning of its inhabitants. For example, AMPS tend to trap longwave radiation near the surface, which results in a warming in and below the cloud layer. The magnitude of this warming scales with the increased concentration of liquid water within the cloud (Solomon et al., 2011) due to absorption (and re-emission) of longwave radiation and can be tens of degrees depending on the horizontal extent and thickness of the clouds; a warming that is often missed by numerical models due to lack of cloud cover or lack of supercooled liquid water within the model. Another important aspect of Arctic weather research is for climate modeling. The complex network of radiative feedback processes in the Arctic (e.g. Albedo, cloud, etc.) results in changes to the net radiation. The ability to accurately forecast AMPS and understanding the underlying microphysical processes can help to reduce the uncertainty within climate models, and help to better understand the role that clouds play in Arctic amplification (Wendisch et al., 2019).

The United States (US) Department of Defense (DoD) also has explicit interest in the Arctic region as a part of the US homeland, an internationally shared region, and a potential corridor for military operations as outlined in the 2019 DoD Arctic Strategy (*Report to Congress Department of Defense Arctic Strategy*, 2019). As changes continue to occur throughout the Arctic such as the diminishing of sea ice, reduced snow cover, and melting of ice sheets, new shipping routes allow increased access to natural resources. Additionally, thawing permafrost and coastal erosion from storm surge can negatively affect infrastructure and complicate the development of new DoD facilities and equipment. Understanding the relationship between Arctic clouds and climate will help to inform DoD decision makers and guide operational decisions in the Arctic.

Operationally, the DoD has an interest in the Arctic due to the adverse effects on aircraft caused by low clouds and the potential for aircraft icing. Low clouds and fog are often observed with reduced visibility and can obscure line of sight for military aviators, which can impact takeoff and landing, air refueling operations, search and rescue missions, intelligence, surveillance, and reconnaissance missions, and many others. Lack of a cloud-free line of sight can also obstruct the use of directed energy weapons, targeting and tracking of enemy aircraft and weapons systems, and elctro-optical and infrared sensors. Aircraft icing conditions have the potential to completely shut down a mission, or, if the mission proceeds, pose a dangerous threat to the aircraft and the personnel in it. Although the severity of icing conditions can vary by region and throughout the year, even mild icing conditions can pose a significant hazard to some aircraft such as unmanned aerial vehicles and remotely piloted aircraft (Williams, 2004). Icing conditions occur in subfreezing temperatures and in the presence of supercooled liquid water, which are commonly observed in the Arctic, rendering the ability to accurately forecast temperature and the temporal and spatial extent of supercooled liquid water paramount. Temperatures well below freezing are commonly observed within the Arctic, and since surface temperature can be drastically warmer (colder) in the presence (absence) of AMPS, it is clear that it is also crucial to accurately forecast Arctic clouds and their physical properties within.

The purpose of this study is to evaluate the ability of four different bulk microphysical parameterization schemes (BMPs) to predict the presence and the properties of a specific case of a persistent, low-level AMPS, which evolved over a 96-hour period. Chapter II of this paper presents a thorough literature review of AMPS properties and a variety of studies which have analyzed AMPS through both observation and modeling studies. A description of the case study and the microphysics schemes used in this research is outlined in chapter III. Chapter IV highlights the results and presents

a discussion of the cloud and boundary layer conditions produced by the four BMPs. Finally, conclusions and opportunities for future work are outlined chapter V.

II. Literature Review

2.1 AMPS Structure and Processes

AMPS can be very unique relative to mid-latitude and tropical stratocumulus. Typically, they are multi-layered and exist within a stable atmospheric profile (Solomon et al., 2011) and can have a wide range of liquid water paths (LWP) ranging from tens to hundreds of $g\,m^{-2}$. In certain atmospheric conditions, AMPS can persist for days to weeks, and the reasons for this are examined by many studies. D. Wang et al. (2020) showed that there exists a very common elevated temperature and moisture inversion near the cloud top, which creates a capped layer. Frequently, supercooled liquid water which is highly concentrated near the top of the cloud layer cools radiatively, while condensation within the cloud releases latent heat into the cloud (A. L. Morrison et al., 2019). This results in colder air above warmer air and instability within the cloud layer, creating turbulent motions that range from tens of m to mm in scale. These turbulent motions simultaneously bring more surface-level moisture into the cloud and entrain moist air from above the cloud layer back into the cloud. In this entrainment region of the cloud, cloud liquid water (water vapor) is transported upward (downward), which furthers the radiative cooling at cloud top. These processes result in a positive feedback loop within AMPS, where radiative cooling produces turbulence, entraining more moisture into the cloud, which eventually produces further cooling, and so on.

A coupled boundary layer in the Arctic implies that surface fluxes of heat and moisture can influence the upper portions of the boundary layer. In a coupled state, there exists a quasi-constant potential temperature throughout the boundary layer down to the surface (Griesche et al., 2021), while a decoupled layer typically occurs when there is a potential temperature inversion, which inhibits the flux of surface

heat and moisture into the boundary layer. Ice-containing clouds in the Arctic were observed to occur more often by a factor of six in coupled layers than in decoupled layers (Griesche et al., 2021). Abrupt instances of large scale subsidence can cause an AMPS cloud to dissipate suddenly, and surface coupling helps to re-build the AMPS layer as soon as that subsidence weakens by supplying heat and moisture to the boundary layer (Neggers et al., 2019). Even in the decoupled case, the updraft region of larger, cloud-scale eddies can supply moisture to further condensation; a process that is internal to the cloud system (Shupe et al., 2008). Radiative cooling is possible near cloud in either the coupled or decoupled case, and this radiative cooling forces direct condensation within non-buoyant parcels near the cloud layer (Solomon et al., 2011).

The modeling of AMPS remains a difficult challenge. Global climate models were shown to have a high sensitivity to the coupling of the surface (Walsh et al., 2002), and in the coupled case, showed stronger temperature variation as a result of the spatial extent of simulated sea ice within the models. Solomon et al. (2011) showed using a high-resolution WRF model that supercooled liquid water was largely underestimated in low-level AMPS. This underestimation resulted in an overall overestimated precipitation rate through the AMPS, and a loss of moisture in the system. Advection sources for moisture were also not captured in this model, which led to a collapse of the cloud system. This collapse led to feedback of errors in radiative budget over the model study area, which led to further errors in cloud cover, and so on. Verlinde et al. (2007) showed that these feedback processes and persistence of AMPS can occur in both strong and weak synoptic forcing, suggesting that cloud structures and properties rely more heavily on microphysics than large-scale dynamical processes.

Inaccurate representation of AMPS in numerical models can have many direct impacts on the simulated Arctic radiation budget as the presence of clouds in the Arctic

is shown to be well correlated with the net upwelling and downwelling of longwave radiation (X. Wang & Key, 2005). Longwave radiation tends to dominate the energy budget for almost half of the year in the Arctic (Chiacchio et al., 2002), and in the presence of clouds, will produce a net warming effect at the surface. The overall cloud radiative effect can change throughout the year, but typically is positive and stronger in the winter months. A key factor in the Arctic-climate system and Arctic Ocean climate is the presence of clouds (Curry et al., 1996), which can significantly affect conditions of the ice-atmosphere-ocean coupling process. Dodson et al. (2020) showed that many numerical prediction models cannot accurately represent the evolution of AMPS which is due in part to the strong dependence on cloud properties in the Arctic region. They also showed that the Arctic System Reanalysis (ASR) had a warm and dry bias of $\sim 1.5\ K$ and $0.06\ g\,kg^{-1}$, which led to lack of production of total water (ice + liquid) and cloud liquid water content and a 4% decrease in relative humidity than was observed. Their analysis also identified that cloud liquid water above 500 m was seldom captured, and only in clouds contained below 500 m was cloud liquid water realistically represented.

Sedlar, Igel, and Telg (2021) conducted a study of atmospheric conditions at Utqiaġvik, AK (Formerly Barrow) over the years 2014 – 2018. They found that although aerosols were a contributing factor in acting as cloud condensation nuclei (CCN), the rate of change of the presence (lack) of aerosols was not a significant factor in the formation (dissipation) of AMPS, as the quantity of aerosols before and after the presence of a cloud remained relatively constant. Rather, they found that the thermodynamic response of the atmosphere was dominated by longwave cooling, and that the changes in relative humidity were loosely negatively correlated with changing temperatures.

The evolution of AMPS and the predicted liquid water path is highly constrained

by the ice number concentration, N_i (Ovchinnikov et al., 2014), in that the production of liquid water is inhibited by excess N_i. Ovchinnikov et al. (2014) analyzed 11 different models in a large eddy simulation (LES) environment of mixed-phase clouds and found that the differences in LWP and ice water path (IWP) can be attributed to the shape of the ice particle size distribution (PSD) used. Schemes that utilized an exponential ice PSD typically underestimated the growth of ice from vapor deposition and overestimated fall speeds, which led to a lower IWP value, on average, than what was predicted from schemes which explicitly predict the PSD. They demonstrated the importance of using an appropriate ice PSD to simulate AMPS as they rely so heavily on the distribution of ice and liquid water.

2.2 Moisture and Precipitation

In the summer and fall seasons in the Arctic, the ice-free ocean near the North Slope of Alaska (NSA) is a large moisture source for AMPS through evaporation. In the winter and spring over the Arctic, heat and moisture fluxes from the ice-covered surface can be low (Li et al., 2020), but leads, which are openings within the ice where the ocean is directly exposed to the atmosphere, can produce heat and moisture fluxes which are up to two orders of magnitude larger than over purely ice-covered surfaces. Li et al. (2020) showed that leads, although only covering a few percent of the total surface area of the Arctic in winter, provide a significant impact to the heat budget of the Arctic boundary layer by supplying heat through the exposure of a relatively warm ocean surface and moisture flux to the surrounding air. This impact is increased near the peripheries of the Arctic Ocean (e.g., the NSA). Leads tend to affect the heat and moisture budget locally, but can also affect the large-scale meteorology and impact the development of low-level clouds when heat and moisture is advected throughout the Arctic.

Readily available moisture and a source of moisture are important factors in cloud development and sustainment, especially in precipitating clouds (A. L. Morrison et al., 2019; Solomon et al., 2011; Verlinde et al., 2007; Solomon et al., 2014). AMPS require initially present moisture and a moisture source, although the specific source of the moisture is not as important as highlighted in a modeling study by Solomon et al. (2014). They showed that when air above the cloud layer is initially drier, it helps support radiative cooling and subsequent turbulent motions, which can transport more moisture from the surface-layer. Radiative cooling can also force direct condensation of particles in non-turbulent air. When air below the cloud is initially drier, water vapor in the mixed-layer is reduced, surface-layer moisture increases, and a loss of moisture through precipitation is reduced. They note that AMPS only decayed when moisture above and below the cloud is reduced, or when there was a large sink of moisture due to too much precipitation removing moisture from the atmosphere.

Rimed precipitation is often overlooked, or assumed to have a minor impact, in the Arctic (Yang et al., 2013). Previous studies of riming in AMPS focused on cases in which LWP was near 100 $g\,m^{-2}$ or more (Fridlind et al., 2007) or in situations of deep cloud systems with tops reaching up to 8 km (Oue et al., 2015). However, Fitch and Garrett (Fitch & Garrett, 2022) showed that a significant amount of riming can occur even in very thin, single-layer AMPS with LWP of less than 50 $g\,m^{-2}$. Through use of a Multi-Angle Snowflake Camera (MASC; ARM Climate Research Facility, 2014; Garrett & Yuter, 2014; Garrett et al., 2012, 2015), they were able to distinguish graupel from aggregate snowflakes. They showed that roughly two-thirds of precipitation particles measured contained significant riming, and that $\sim 20\%$ were heavily rimed. This was attributed to a weak boundary layer inversion and strong cloud top cooling, which resulted in updrafts sufficient to produce riming for roughly half of the rimed precipitation particles. They note that the evidence for this attribution is weak and

will require both real-world and idealized modeling studies to further substantiate their results. Riming in AMPS is important because it is an efficient sink of liquid and aerosols from the Arctic boundary layer through precipitation, and consequently results in changes to the AMPS structure and ultimately the surface energy budget over the Arctic (Fitch & Garrett, 2022).

2.3 Aerosols as CCN and INP

The interaction between aerosols and the development of cloud particles is still a prominent subject of ongoing research. Solomon et al. (2018) conducted an LES study of the relationship between aerosols and cloud dynamics of AMPS for a specific case at Oliktok which occurred in April, 2015. They found that perturbations in ice nucleating particles (INPs) had a dominant effect over perturbations in CCN. This was because increasing the number of INPs within AMPS produced a "glaciation effect" (Murray et al., 2012), where there was a rapid depletion of cloud liquid. Solomon et al. (2018) found that there was a strong, nonlinear increase to LWP through increases in CCN which was a direct result of the average cloud droplet size decrease, an increase in longwave emissivity, and cloud top cooling. A ten-fold increase in INPs resulted in a large increase to IWP, with a moderate decrease to LWP, while a two-fold increase to INPs resulted in a moderate increase to IWP, with a large decrease in LWP. The increased concentrations of CCN above cloud top and increased INPs within the mixed-layer led to the maintenance of cloud liquid, which drove cloud-top radiative cooling, and was essential for the persistence of the AMPS examined. Finally, the thinning of the liquid layer in the cloud coincident with increased concentrations of INPs resulted in a rapid glaciation of the cloud, and caused the cloud to radiate as a "grey body", which lessened cloud-top radiative cooling and subsequent buoyant overturning.

One important aerosol type is marine organic aerosols (MOA), which are emitted over almost three-quarters of Earth's surface through sea spray and can have a large impact on the surface budget and regional climate (Zhao et al., 2021). Although MOA are commonly thought to be transported long distances into the Arctic during winter and early spring (Quinn et al., 2002), a recent study in 2019 showed that the dominant source of MOA in these seasons are from leads (Kirpes et al., 2019), which are expected to become more significant under a warming climate. These aerosols can have a large impact on the radiative properties of mixed-phased clouds, especially at high-latitude regions, and act as an important INP. Zhao et al. (2021) showed that INPs consisting of MOA are the main source of primary ice nucleation below the 400 hPa pressure level over the Southern Ocean and Arctic Boundary layer, while dust INPs are more common elsewhere. The treatment of MOA as an INP proved to be a significant form of ice nucleation for immersion freezing.

In addition to organic aerosols, anthropogenic aerosols also impact AMPS development. Maahn, Goren, Shupe, and de Boer (2021) conducted a study with data between 2006 and 2019 to study the effects of anthropogenic aerosol emissions (sulfur dioxide) on cloud and condensation properties of Arctic clouds. They analyzed data from the Moderate Resolution Imaging Spectroradiometer (MODIS) in an area between Utqiagvik and Deadhorse, AK (note Oliktok is between these two regions, although closer to Deadhorse). They found that when the primary wind direction was from the east-northeast to the east-southeast these locations were downstream of a major source of sulfur dioxide emissions. During this wind regime, they found that the average cloud liquid droplet radius over much of the region decreased, and number concentration of cloud droplets increased as far as 100 km downstream. This result is important because the average optical depth of clouds over this portion of the Arctic was increased and there was a subsequent increase in upwelling (downwelling)

shortwave and longwave (longwave) radiation (Maahn et al., 2021). This change to the radiative properties is in direct support of the mechanisms which help to maintain AMPS, as stronger radiative cooling at cloud top enhances the condensation production and furthers cloud liquid water production.

Of the various types of aerosols which may be present at any given point and time within the Arctic, Bulatovic et al. (2021) showed that Aitken mode particles (diameters of 25-80 nm) are important to AMPS. They showed that, even in low concentrations (10-20 cm^{-3}) of accumulation mode aerosols (diameters of 100s of nm) and when particles have a low hygroscopicity (hygroscopicity parameter, k=0.1), Aitken mode particles can significantly affect the radiative properties and microphysics and help to maintain AMPS. The presence of Aitken mode aerosols coincident with particles of higher hygroscopicity resulted in more cloud liquid. However, when there were higher ice fractions, the Aitken mode particles had a significantly smaller impact on cloud liquid.

2.4 Microphysics

There are a number of challenges when trying to accurately simulate condensation and precipitation processes within a cloud. The two main challenges when attempting to resolve microphysics in a model are the inability to model all possible particles within a cloud, and the uncertainty due to knowledge gaps of certain microphysical processes (A. L. Morrison et al., 2019). Due to the vast number of particles in even the smallest of clouds and sizes ranging from sub-micron to centimeters, it would be computationally irresponsible to attempt to explicitly resolve condensation and precipitation processes. For this reason, microphysics schemes are implemented in numerical weather prediction models using statistical methods to parameterize subgrid-scale processes. This generally allows for a relaxation on com-

putational resources while maintaining a statistically realistic representation of clouds in the atmosphere.

There are two main types of microphysics schemes used in numerical models: BMPs and spectral (bin) microphysics (SBM). BMPs typically use an empirical function to assume the size distribution of hydrometeors, which does not change throughout the simulation. BMPs can consist of one-moment (number concentration; e.g. Hong, Noh, and Dudhia (2006)), two-moment (number concentration and mass mixing ratio; e.g. H. Morrison, Thompson, and Tatarskii (2009)), and three-moment (number concentration, mass mixing ratio, and radar reflectivity; e.g. Milbrandt and Yau (2005)). These prognostic variables generally allow for computational efficiency, but can cause limitations such as errors in the spatial distribution of different particle sizes (Yin et al., 2017). SBM describes the size distribution of each type of hydrometeor and CCN using tens to hundreds of mass bins. This organization of hydrometeors provides the potential for a better spatial distribution of particles, but can be computationally intensive as compared with the simpler BMP concept (Yin et al., 2017).

The simulation of AMPS can be sensitive to which microphysics scheme is chosen to represent. H. Morrison et al. (2009) showed, performing a sensitivity test of several different models, that schemes which use a double-moment were better able to capture the LWP than schemes which only use a single-moment. They attributed this to the fact that many of the single-moment schemes, which only accounts for the mass mixing ratios of the various cloud and precipitation particles, use a temperature threshold for conversion of liquid to ice, and in many cases that conversion happens much too quickly. The conversion from liquid to ice was still too rapid even among the double-moment schemes, which account for mass mixing ratio and number concentration, and in general the models used produced unrealistically large amounts of ice within

the cloud layers. H. Morrison et al. (2009) also showed via sensitivity tests that increasing the vertical levels within the models tended to generate more LWP, as it allowed for better convergence within the simulations. This is consistent with the LES modeling study by Solomon et al. (2014), which showed that there was more moisture produced as the vertical and horizontal resolutions of the model were increased. For these reasons, LES (or equivalent) should be used to study AMPS as opposed to the coarser resolution of many operational models (tens of km horizontal and hundreds of m vertical).

III. Methodology

3.1 Case Study

The event analyzed in this study took place in late April 2017 near Oliktok Point, Alaska (hereafter simply Oliktok). A mixed-phase cloud became present on the 25th and persisted until at least the 28th. This study examines a window within the AMPS event from 1200 UTC on the 26th to 1200 UTC on the 27th at Oliktok. A snapshot of cloud coverage at 0000 UTC on the 27th is shown in Figure 1. The horizontal extent of the cloudy areas covers much of the frozen Arctic ocean north of Alaska, which extends several tens of kilometers south, and hundreds of kilometers east and west of Oliktok. Observation of cloud and precipitation properties at Oliktok were recorded by a 3-channel microwave radiometer (MWR3C; M. P. Cadeddu et al., 2013; M. Cadeddu, 2021). Cloud top height, mean Doppler velocity, and reflectivity were recorded by a Ka-band Atmospheric Radiation Measurement (ARM) Zenith Radar (KAZR; ARM Climate Research Facility, 2015; Clothiaux et al., 2000), and cloud base height was retrieved from a ceilometer (Morris, 2016). The surface and boundary layer conditions were measured using surface observations (ARM Climate Research Facility, 2013c), balloon (ARM Climate Research Facility, 2013a), and interpolated (ARM Climate Research Facility, 2013b) soundings. Confidence in the interpolated soundings is higher when the interpolation valid time is closest to the valid time of the balloon observations, which were taken within a few minutes of 1730 and 2330 UTC each day.

High pressure existed just to the north of the NSA, moving to the east-southeast over this time frame as depicted by the yellow contours in Figure 2, and winds remained between 4 and 7 $m\,s^{-1}$ from the east-northeast. Initial LWP at Oliktok was 150 $g\,m^{-2}$ and cloud top was near 1 km, above which a strong temperature and mod-

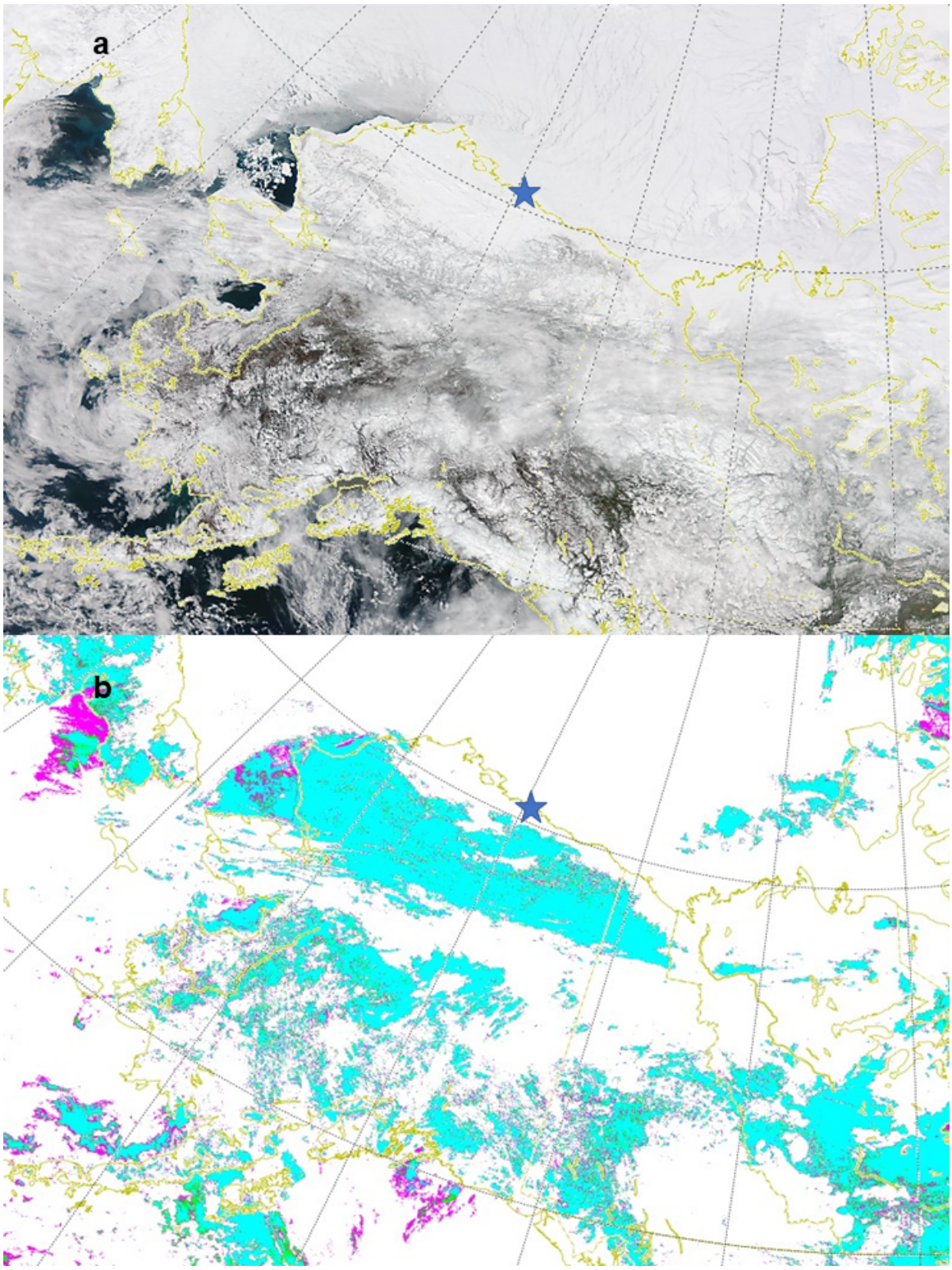

Figure 1. Cloud coverage over Alaska at 0000 UTC on the 27th retrieved from the Visible Infrared Imaging Radiometer Suite (VIIRS). (a) shows the visible satellite retrieval. (b) shows confidence where white (blue) is confident cloudy (clear) and other colors depict areas of uncertain cloud coverage.

erate specific humidity inversion existed. Precipitation of any kind was minimal to non-existent during this initial period and radar reflectivity varied between -30 to -10 dBZ (0 dBZ) coincident with smaller-sized cloud particles (larger, rimed precipitation particles). Between 1200 and 2359 UTC on the 26th, the LWP decreased steadily down to roughly $50g\,m^{-2}$. During this same time the cloud height and inversion base decreased down to 0.5 km. Moderately and heavily rimed precipitation was observed shortly after and continued through 1200 UTC on the 27th.

This study analyzes the general accuracy of the WRF-ARW at LES scales to produce the AMPS cloud of interest, its timing, and capture the decreased LWP prior to precipitation. Simulated mixing ratios of liquid, ice, snow, and graupel are analyzed. The resultant vertical atmospheric profiles and boundary layer conditions are also examined. A sensitivity test is conducted for four microphysics schemes – Predicted Particle Properties (P3), Thompson, Morrison, and WRF Single-Moment 6-Class (WSM6). A description of each scheme is covered in section 3.4 and outlined in Table 2.

3.2 Computing Resources

This study utilizes the high-performance computing (HPC) capabilities of the National Centers for Atmospheric Research (NCAR) Computational and Information Systems Laboratory (CISL; *Computational and Information Systems Laboratory*, 2019). A total of 200,000 core-hours were allotted for this study for use on the Cheyenne HPC. WRF-ARW was compiled to simulate a real case. Due to the domain-size restrictions on allowed processor usage, 900 processors were used for each model run. Output data was downloaded locally, and written to Network Common Data Form (netCDF) files. Post processing and plotting of output data is analyzed using Spyder, a scientific Python development environment.

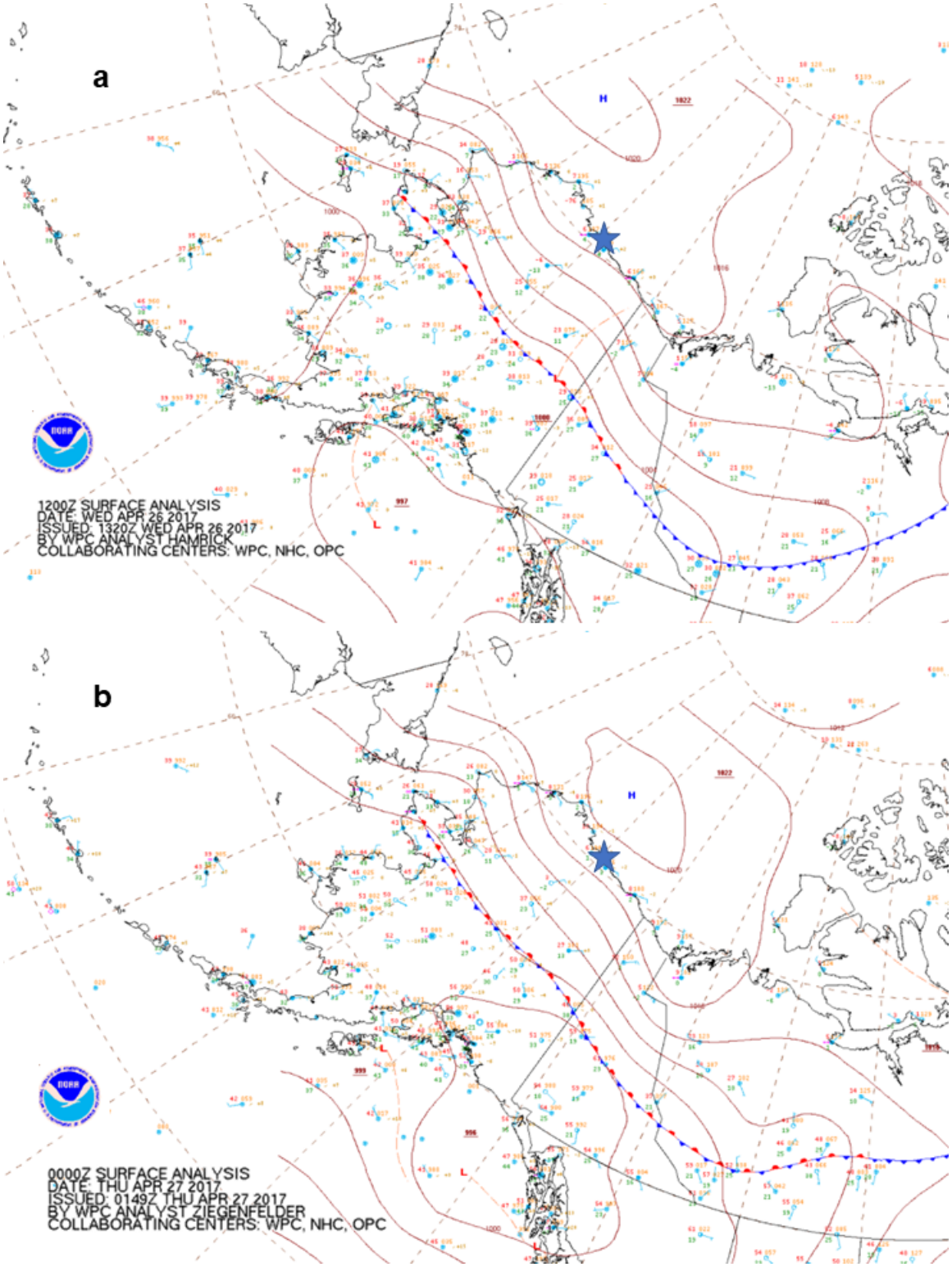

Figure 2. Surface analysis for (a) 1200 UTC on the 26th and (b) 0000 UTC on the 27th over Alaska produced by the National Weather Service (NWS). The blue star shows the location of Oliktok.

3.3 Model Setup

The model used in this study is the WRF-ARW v4.3 (Skamarock et al., 2021). WRF is an open-source, community atmospheric model that has been in use since the latter part of the 20th century, and was designed to bridge the gap between research and operations in numerical weather prediction. It is equipped with a fully-compressible, nonhydrostatic equations solver, and the user is able to specify various parameters to include physics schemes, numerics/dynamics, initialization routines, data assimilation packages, and more. WRF is also efficient for computing on devices from personal, at-home computers to large supercomputers and can be used for a wide array of applications. In research, WRF can be configured for a real case to produce simulations based on actual atmospheric conditions (observation or analysis) or from idealized conditions. The readily-configurable and ease of use of WRF, along with the ability to nest down to smaller domains and run at LES scales is the primary reason for its use in this study.

A real case is simulated with forcing from the European Center for Medium-Range Weather Forecasts (ECMWF) Fifth Generation Reanalysis (ERA5; Hersbach et al., 2020) data ingested at six-hour intervals from 0000 UTC on 26 April to 1200 UTC on 27 April, 2017. The ERA5 replaced the older version of ERA-Interim reanalysis, and one of the main improvements in ERA5 relative to ERA-Interim is a higher horizontal resolution of 31 km instead of 80 km. ERA5 also has improved the temperature, winds, and humidity within the troposphere compared to its predecessor (Hersbach et al., 2020), and is able to represent low frequency variability especially well. ERA5 is chosen as the reanalysis dataset to use for this study as it has been shown to perform well in the Arctic (Graham et al., 2019), where there is a lack of observational data relative to many other geographical locations.

Three nested domains (four total; shown in Figure 3) are centered around Oliktok

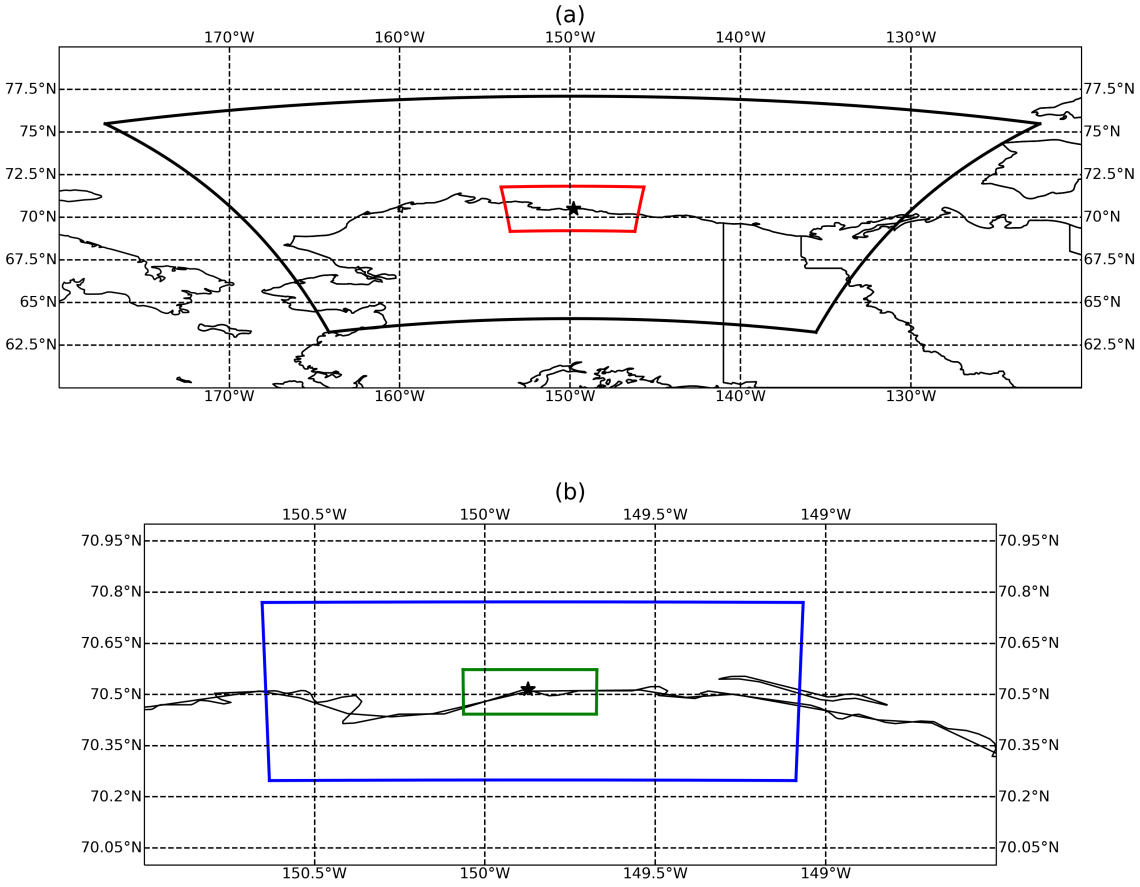

Figure 3. Domain boundaries specified in WRF for domain one (thick, black lines), two (red lines), three (blue lines), and four (green lines). The black star shows the location of Oliktok.

Point with horizontal resolutions of 5 km, 1 km, 200 m, and 50 m from the outermost to innermost domain, which are hereafter referred to as domains one, two, three, and four respectively. Each domain contains 301 x 301 grid points in the east-west and north-south directions with 101 vertical levels. Eta levels are specified within the model to ensure that there are 64 vertical grid points below 2 km. The highest vertical resolution below 2 km is 26 m at cloud base, climbing to 32 m at the top of the cloud layer. Vertical resolutions above 2 km span from 100 m up to $\sim$ 1 km at model top. The higher vertical resolution in the lower levels allows for more tightly packed grid points around the cloud layer to better capture the inversion above cloud top, and better resolve vertical motions which influence cloud development. Ideally, a higher vertical resolutions should be used (200+ vertical levels), but computational constraints demanded fewer vertical levels to ensure all four simulations would be completed. Increasing the vertical resolution in WRF also requires decreasing the time step in the model to avoid any Courant-Friedrichs-Lewy (CFL) violations, which can occur when flows within the model move past adjacent grid points quicker than models time step.

Domains one and two begin execution at 0000 UTC on 26 April as outlined in Table 1, allowing for at least 12 hours of "spin up" time prior to initial cloud formation. Domains three and four begin at 1200 UTC on 26 April, giving two hours of spin up prior to the decrease in LWP and 12 hours prior to the onset of rimed precipitation. The timestep for each domain, in seconds, is 8, 4, 1, and 0.25 for domains one, two, three, and four, respectively. Domains one and two were limited on how large the time step could be by the vertical resolution. Initial test runs utilized larger time steps for domains one and two, but due to wind speed and advection occurring too quickly from one grid point to another, those runs resulted in CFL violations. To avoid any CFL violations within the model, a lower time step was needed to ensure that the

Table 1. A quick reference for the main details of each domain.

	Domain 1	Domain 2	Domain 3	Domain 4
Horizontal Resolution (m)	5000	1000	200	50
Grid Points E-W	301	301	301	301
Grid Points N-S	301	301	301	301
Grid Points Vertical	101	101	101	101
Start Time (UTC on the 26th)	0000	0000	1200	1200
End Time (UTC on the 27th)	1200	1200	1200	1200
Time Step (s)	8	4	1	0.25

model was able to explicitly resolve vertical motions without becoming unstable.

Physics options used in this model follow closely to Solomon et al. (2011) and consist of the Yonsei University Scheme (YSU; Hong et al., 2006) for planetary boundary layer, the Community Atmospheric Model (CAM) Short and Longwave Radiation Schemes (Collins et al., 2004), the Unified Noah Land Surface Model (Tewari et al., 2004) for surface physics, and the Revised MM5 Scheme (Jiménez et al., 2012) for the surface layer evolution. Subgrid-scale turbulence is parameterized using a sixth order diffusion and a 1.5 turbulent kinetic energy (TKE) prediction scheme for domains two, three, and four. A cumulus parameterization scheme is not used as even the coarsest resolution of domain one allows for the generation of explicit convection.

Table 2. A quick reference for the main details and differences in each MP Scheme. Note that P3 groups graupel and snow into the ice category, leaving two "less" species than the other three schemes.

	P3	Thompson	Morrison	WSM6
Moments	2	1 (2 ice)	2	1
Number of Species	4	6	6	6
Ice Phase Category	1	3	3	3
Aerosol Concentration (cm^{-3})	300	0.5	72	N/A
CCN (cm^{-3})	200	100	250	N/A

3.4 Microphysics Schemes

3.4.1 P3

The P3 scheme (hereafter simply P3) is a double-moment, single ice species microphysics scheme which prognoses four ice mixing ratio variables: total mass, rimed mass, rime volume, and number concentration (H. Morrison & Milbrandt, 2015). Other predicted variables in P3 include the mixing ratios and number concentrations of cloud water, water vapor, and rain. The goal of this scheme is to parameterize the many complex relationships between ice particle shape, size, and density, while also maintaining a realistic representation of the evolution of ice particle characteristics. Rather than pre-define ice particles as cloud ice, graupel, snow, etc. like many other schemes do, P3 seeks to use a single ice phase category with various properties, from which more predicted properties can be derived such as rime mass fraction, bulk density, mean particle size, terminal velocity, and more.

Within P3, smaller ice particles are represented as spheres with a density of 917 $kg\,m^{-3}$, and larger ice particles are generally not spherical and have a lower density

than a spherical particle of the same maximum dimension. Therefore, the density of larger particles is defined as the particle mass divided by the volume of a sphere with the same maximum dimension. When an ice particle undergoes riming in P3, the crevices of the particle are "filled in" first, and when the particle is fully "filled in", it is considered graupel. Another consideration is that P3 allows for growth of ice particles by allowing more rime mass to accumulate on the peripheries of the particle before the particle mass is equal to that of graupel. Mass-weighted fall speeds are proportional to the projected areas of a particle. For spherical particles, a simple cross-sectional area calculation of $\frac{\pi}{4}D^2$ is used. For nonspherical particles, an empirical relationship is applied which was derived from observations. P3 also uses a default constant aerosol concentration of 300 cm^{-3} and a mean size of 0.05 μm. The CCN concentration is set to 200 cm^{-3}.

The main differences in P3 from other schemes allow it to navigate around the use of poorly constrained auto conversion thresholds and represent a continuum of particle properties, rather than categorize them. This makes the ability to represent ice particles within the model more accurate, while maintaining computational efficiency as it prognoses only a small number of variables relative to other bulk schemes.

3.4.2 Thompson

The Thompson scheme (hereafter simply Thompson) is one of the first BMPs to utilize exponential and gamma distributions to represent the assumed snow size distribution as a function of ice water content and temperature (Thompson et al., 2008). Thompson predicts the mixing ratios of five different liquid and ice species: cloud water, rain, cloud ice, snow, and graupel. Thompson also predicts the number concentration of cloud ice, making it a single-moment scheme with a double-moment ice phase. This allows for a higher degree of accuracy when predicting ice particle prop-

erties, while maintaining computational efficiency, as full double-moment schemes can be costly on computing resources, which limits their use in real-time numerical prediction models.

Each hydrometeor species within Thompson is specified by a generalized gamma distribution and transitions between species is specified by a lookup table derived from observations. Sensitivity experiments conducted by Thompson et al. (2008) showed that the production of supercooled liquid water droplets is highly affected by the sphericity and constant density assumptions of snow. Therefore, snow is assumed to be nonspherical and its density varies inversely with its diameter. One of the snow distribution assumptions is that snow forms by vapor depositional growth onto cloud ice particles. An arbitrary threshold size of 200 μm is used to transition growing cloud ice to snow, which allows for smaller ice crystals to coexist with falling snow.

Thompson is considered an "aerosol aware" microphysics scheme, as its aerosol concentration is not set to a constant (Thompson & Eidhammer, 2014). Aerosols allow for the explicit cloud droplet activation and ice nucleation. Initial aerosol concentration in Thompson was set to 0.5 cm^{-3} and adjusted via advection through the simulation and CCN was initially set to 100 cm^{-3}. As aerosols are allowed to change throughout the simulation due to advection, certain areas might contain a higher aerosol concentration in any given timestep than in previous one. Thompson uses this concept in its parameterizations because increased aerosol concentration allows for more numerous, smaller size cloud droplets to exist (although Thompson does not explicitly predict number concentration for cloud liquid), and delays precipitation development. This also results in an increased cloud albedo effect, and more subtle longwave radiation effects. Thompson categorizes aerosols as "water friendly" or "ice friendly", and cloud droplets nucleate from explicit aerosol number concentrations using a lookup table derived from the model's predicted temperature, vertical

velocity, and number of available aerosols. Within Thompson, when ice is allowed to grow by vapor deposition, the nucleation of new cloud droplets is halted for the given timestep.

3.4.3 Morrison

The Morrison scheme (hereafter simply Morrison) is a double-moment microphysics scheme which predicts the mixing ratio and number concentrations of five species: cloud droplets, cloud ice, snow, rain, and graupel (H. Morrison et al., 2009). A gamma function is used to represent the cloud and precipitation particle size distributions, and all particles are assumed to be spherical for simplicity. Unlike P3 and similar to Thompson, Morrison pre-defines the categories for each hydrometeor species and uses auto conversion to convert from one species to another (e.g. cloud water to ice or rain) set by a threshold and found in a lookup table.

The minimum mixing ratios required for conversion are as follows: 0.1 $g\,kg^{-1}$ of each rain and snow are required to produce graupel from collisions between rain and snow, 0.1 $g\,kg^{-1}$ of snow and 0.5 $g\,kg^{-1}$ of cloud droplets are required to produce graupel from collisions between snow and cloud droplets, and 0.1 $g\,kg^{-1}$ of each rain and ice are required to produce graupel from collisions between rain and cloud ice. All changes in the phase of one species are equal to the changes of another from which it transitioned (e.g., increase in rain due to melting is equal to decrease in snow or graupel). Aerosol concentration was set to 72 cm^{-3} and CCN was set to 250 cm^{-3}.

3.4.4 WSM6

The WSM6 scheme (hereafter simply WSM6) is a single-moment microphysics scheme which only predicts the mixing ratios of water vapor, cloud water, cloud ice, rain, snow, and graupel (Hong et al., 2006). WSM6 pre-defines each hydrometeor

species into each of these categories using various thresholds and auto conversion to convert between different phases. An exponential distribution is assumed for graupel particles. It is assumed that the ice nuclei number concentration is a function of temperature and the ice crystal number concentration is a function of the amount of ice.

Although a much simpler scheme, WSM6 does have its relative advantages over the other three schemes chosen for this study. The main advantage that WSM6 possesses is computational efficiency (Hong et al., 2006). Since number concentrations are not predicted, but rather inferred from the mass mixing ratios and size distributions, there are less steps to calculate in each iteration of the model, resulting in less overall time to run the full model compared to P3, Thompson, and Morrison. The magnitudes of these timestep differences in this study are discussed in the results section.

The main reason behind each of the microphysics schemes chosen for this study is to try and highlight which types of schemes might best represent a case of rimed precipitation from AMPS with low liquid water paths. Here a full double-moment scheme with predefined categories (Morrison), a double-moment scheme with a continuous ice phase category (P3), a single-moment scheme with a double-moment ice species and predefined categories (Thompson), and a full single-moment scheme (WSM6) are analyzed. Ideally, more schemes would be analyzed to better compare the differences in producing the AMPS of interest, but computational resource limitations were a preventative factor. A total of 200,000 core hours were granted by CISL for this study, and each model run cost $\sim$ 45,000 core hours, leaving room for only four microphysics schemes to be tested without having to request additional computational time on the Cheyenne HPC.

3.5 Model and Observation Output

The output from each model was written in hourly intervals to netCDF format. From there, all of the data is extracted into NumPy arrays using Spyder. Each output variable in domain four was averaged horizontally, and that average is used to represent the conditions from the 50 m resolution run at Oliktok. Analysis of conditions at Oliktok for domains one, two, and three is represented by the closest point in latitude and longitude from the model output. The output data from observations is interpolated onto a height grid matching that of the model data utilizing a linear interpolation tool within Python. Observations with a relatively low temporal variability are extracted at the closest hourly value to compare to model output. These variables include LWP, precipitable water vapor (PWV), optical depth, surface temperature, surface pressure, cloud base height, and cloud top height. Higher temporal variability observations such as precipitation rate and reflectivity are taken as the average of the prior hour to compare to model output (e.g. the 1800 UTC precipitation rate is the average from 1700-1800 UTC).

Certain non-standard variables needed to be calculated from available model output variables, such as the liquid, ice, snow, and graupel water path (LWP, IWP, SWP, GWP), which are given by the equation:

$$WaterPath = \sum_{0}^{p=p_0} \frac{r_L \Delta p}{g} \tag{1}$$

Where p is the pressure at a given level in hPa, p_o is the pressure at the lowest level in hPa, r_L is the mixing ratio of either liquid, ice, snow, or graupel in $g\,kg^{-1}$, Δp is the change in pressure from one level to the next in hPa, and g is the acceleration due to gravity of 9.81 $m\,s^{-2}$. Since P3 only contains a single ice category, ice water path in P3 is compared to the "total ice" water path from the other three MP schemes,

which is calculated by simply adding the ice, snow, and graupel water paths together. This is hereafter referred to as total ice water path (TIWP). Precipitation data from model output is given in total accumulated at hourly intervals. To compare this data to the output from observation (given in $mm\,hr^{-1}$), a gradient is computed using a second order, central differencing in the interior points of the precipitation arrays and either a first or second order one-side difference at the boundaries. This particular use of gradient calculation results in a slightly erroneous first index from model output (1200 UTC on the 26th). All indexes after the first in the model output arrays are calculated as $P[i+1] - P[i]$, where P is the precipitation array, and i is the index within that array (0-24). This technique is not ideal in most scenarios, but it was computationally efficient and simplified plotting the data. Since each model run requires spin-up time, the zero-hour model output is not analyzed in depth here, justifying use of this gradient technique, and allowing the option to keep the precipitation arrays from model output the same size as from observation to easily compare all hours.

IV. Analysis

4.1 Results

4.1.1 Cloud Structure

Figure 4 shows cloud fraction output from each microphysics scheme with overlaid cloud top and base heights from observation. P3 was able to capture the general shape of the cloud structure, but lacked in the vertical extent of the cloud. It was also able to capture the decreasing cloud top height trend over the last $\sim$ 12 hours of the model run and represented cloud base fairly well. The cloud produced by P3 was almost entirely ice and snow particles as shown in Figure 5, with very little liquid water highlighted in Figure 6, and no riming (rime mass mixing ratio; not shown) produced. The captured decrease in cloud top height was likely not due to accurate resolving of the cloud and condensation microphysics within P3, but rather the early dissipation of the cloud. Since P3 produced essentially an entirely ice-filled cloud, there was a lack of radiative cooling at cloud top relative to a cloud with significant supercooled liquid water, and consequently, a lack of vertical motions and entrainment of moisture into the cloud layer.

Thompson was able to capture more of a vertical extent to the cloud feature, although slightly under forecast (over-forecast) cloud base (top). Thompson did not capture the decreasing cloud top height quite so well, with the only decrease occurring during the last two-to-three hours of model simulation. The cloud produced in Thompson was almost entirely liquid water, with relatively small amounts of ice and snow, and no riming (graupel; not shown). The sustainment of the cloud produced by Thompson is likely due to the larger amounts of cloud liquid water, which resulted in stronger radiative cooling at cloud top, entraining more moisture into the cloud which is evident in Figure 7.

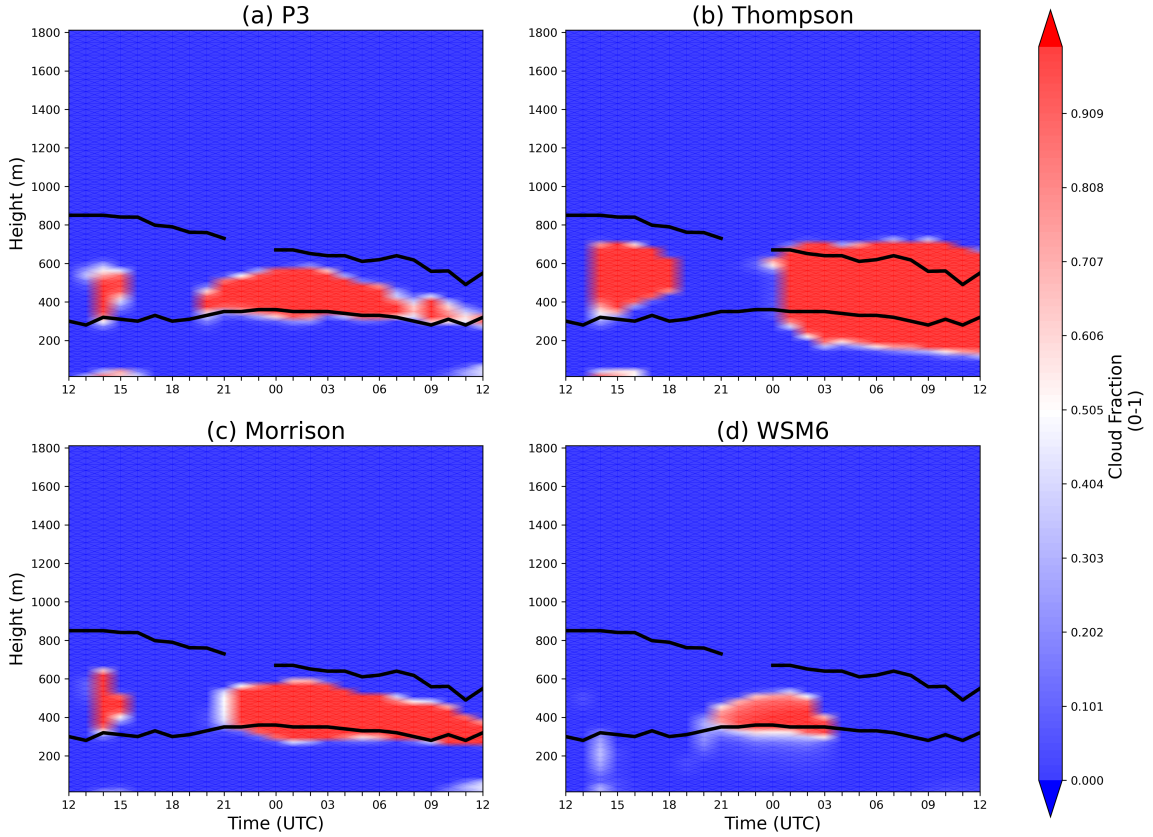

Figure 4. Time-height cross section of cloud fraction (range of 0-1) produced by (a) P3, (b) Thompson, (c) Morrison, and (d) WSM6 at Oliktok from 1200 UTC on the 26th to 1200 UTC on the 27th. Solid black lines show the observed cloud base and top heights.

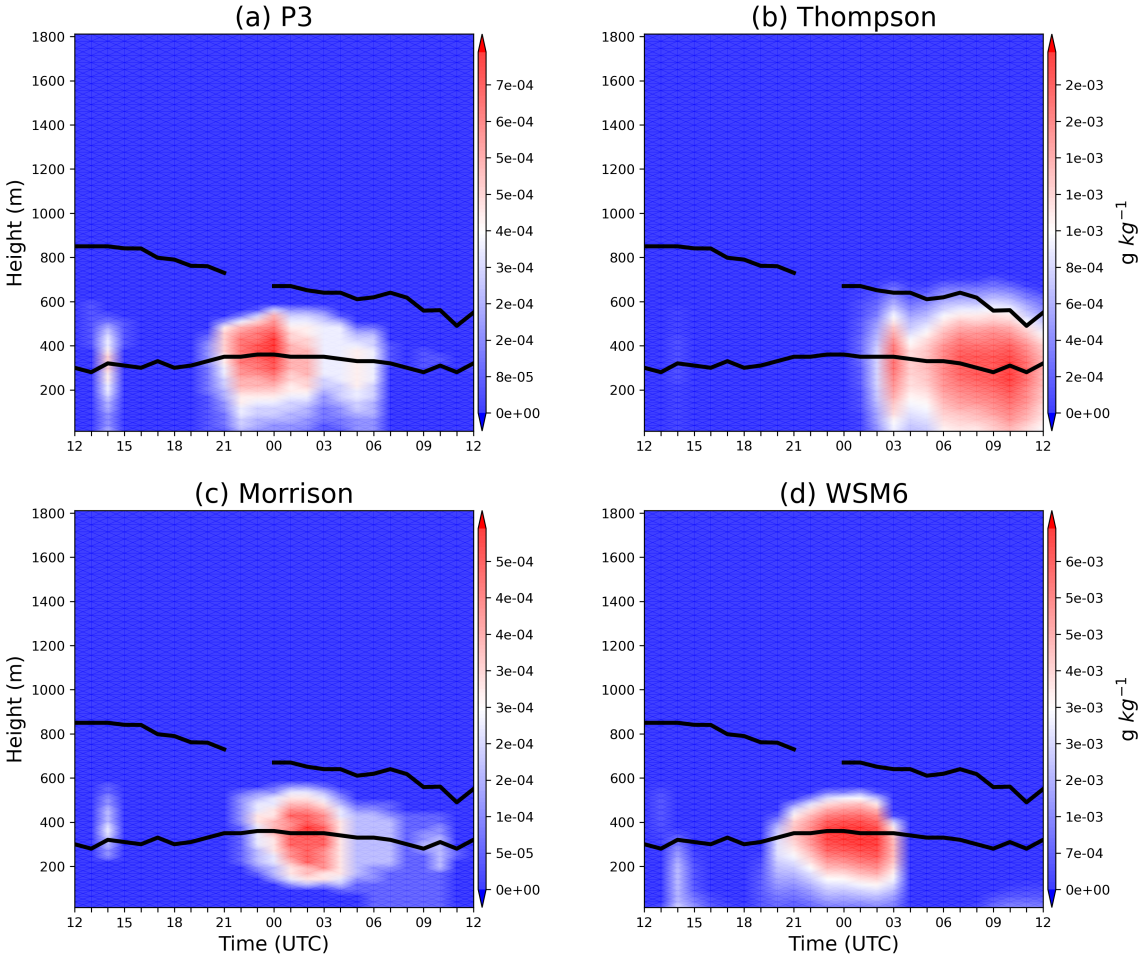

Figure 5. Time-height cross section of ice plus snow mixing ratio ($g\,kg^{-1}$) produced by (a) P3, (b) Thompson, (c) Morrison, and (d) WSM6 at Oliktok from 1200 UTC on the 26th to 1200 UTC on the 27th. Solid black lines show the observed cloud base and top heights.

Morrison performed similarly to P3 in representing the overall structure of the cloud, which captured well the decreasing cloud top height through the last ~ 12 hours of simulation. However, Morrison performed slightly better than the P3 scheme on the vertical extent of the cloud, and captured the total thickness of the cloud well, but forecast cloud base and top $\sim 100\ m$ lower than was observed. The cloud produced in Morrison was almost entirely ice particles, with very little liquid water and snow, and no riming (graupel; not shown). The decrease in cloud top height in Morrison is likely similar to P3, and is likely a result of early cloud dissipation, rather than an accurate representation of the observed event.

WSM6 struggled to capture the overall structure of the cloud, producing only a short lived, thin ice cloud which formed and dissipated in just 5 hours of simulation time. Of the cloud that was produced in WSM6, the cloud base was well forecast, but lacked on the vertical extent of the cloud. The cloud produced in WSM6 was entirely ice particles, with very little snow, no liquid water and no riming (graupel; not shown). The quick formation and dissipation in WSM6 is likely due to rapid ice production within the model, and precipitation, which removed moisture from the system and ultimately led to the quick collapse of the cloud system.

4.1.2 Liquid and Total Ice Production

The only scheme to produce a significant liquid water path was Thompson as shown in Figure 8. There was initially no liquid water present, and none produced, until ~ 12 hours into the simulation, after which the Thompson scheme produced up to $\sim 50\ g\,m^{-2}$ of liquid water, which increased through the end of the simulation. Thompson's liquid water was highly concentrated near the top of the cloud layer as shown in Figure 6, which tapered off down toward cloud base. The values of LWP in the Thompson scheme match well to observations over the last 10 hours

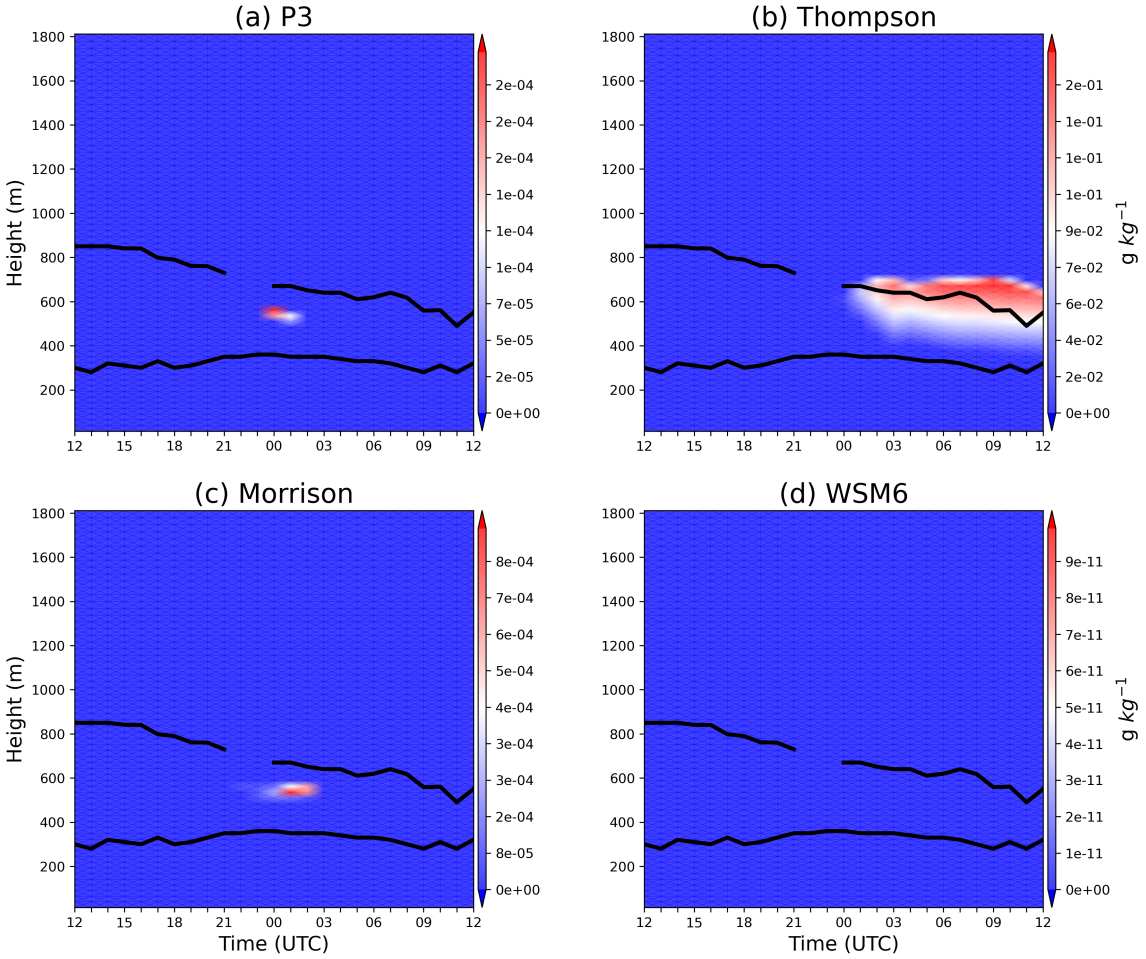

Figure 6. Time-height cross section of cloud liquid mixing ratio ($g\,kg^{-1}$) produced by (a) P3, (b) Thompson, (c) Morrison, and (d) WSM6 at Oliktok from 1200 UTC on the 26th to 1200 UTC on the 27th. Solid black lines show the observed cloud base and top heights.

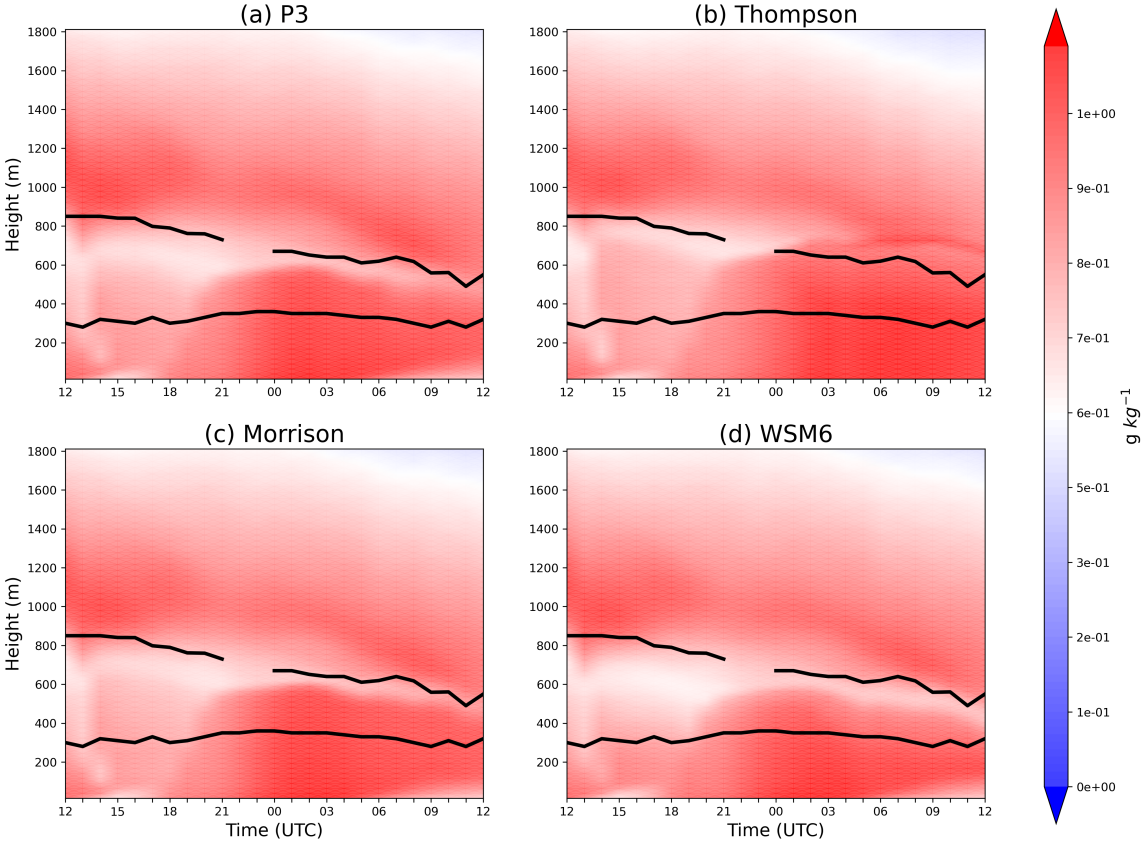

Figure 7. Time-height cross section of water vapor mixing ratio ($g\,kg^{-1}$) produced by (a) P3, (b) Thompson, (c) Morrison, and (d) WSM6 at Oliktok from 1200 UTC on the 26th to 1200 UTC on the 27th. Solid black lines show the observed cloud base and top heights.

of simulation, although the trend is in the wrong direction. Both P3 and Morrison produced a maximum LWP of less than 0.1 $g\,m^{-2}$, and WSM6 produced no liquid water at all. The little amount of liquid water that did exist in P3 and Morrison occurred near cloud top for less than two hours at the beginning of cloud formation.

Figure 9 shows TIWP generated by each model. Thompson produced a TIWP with maximum values 1.5 $g\,m^{-2}$, the overwhelming majority of which was snow. The concentration of total ice in Thompson was contained to the last few hours of simulation near the cloud top, and existing only within 600-700 m above the ground. P3 produced a TIWP of up to 0.4 $g\,m^{-2}$, which was concentrated near the middle of the cloud layer, tapering off just above (below) cloud top (base), and between 2200 to 0600 UTC of the simulation. Morrison followed a similar pattern to the P3 scheme, although TIWP values topped out around 0.3 $g\,m^{-2}$. Concentrations of total ice in Morrison were more or less evenly distributed through the cloud layer. WSM6 produced the most TIWP of all of the microphysics schemes, with a maximum of 3.25 $g\,m^{-2}$. The concentration of cloud ice in WSM6 was evenly distributed throughout the cloud layer, with very small amounts near cloud top and base.

None of the microphysics schemes produced any rimed cloud particles at Oliktok. For Thompson, Morrison, and WSM6, the graupel mixing ratio was a constant zero through the duration of the simulation. For P3, the rime mass mixing ratio also remained zero throughout the simulation. Morrison and WSM6 produced small amounts of snow mixing ratios, leading to maximum SWPs of 0.2 and 0.02 $g\,m^{-2}$, respectively. The concentration of snow particles within Morrison were evenly distributed throughout the cloud layer, existing only in the beginning of cloud formation at $\sim$ 21 UTC, and tapering off quickly at about six hours after. The concentration of snow particles in WSM6 was evenly distributed in the lower two-thirds of the cloud layer, and existed only between one hour after (before) cloud formation (dissipation).

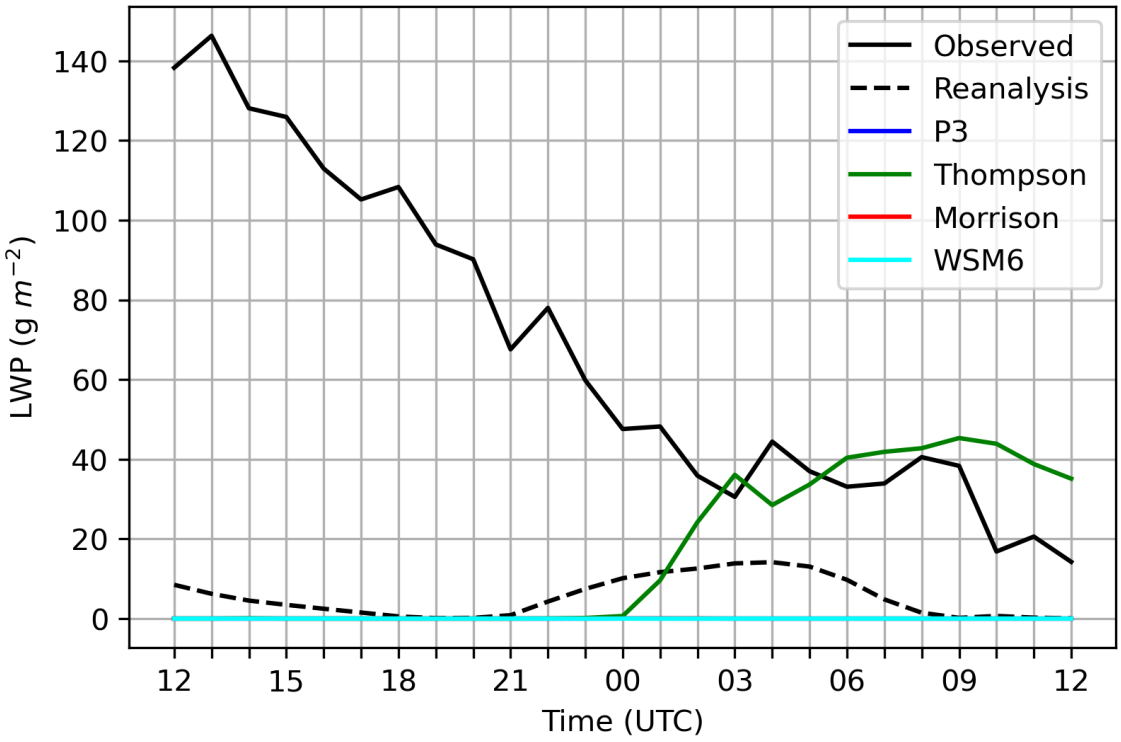

Figure 8. LWP observed and produced by P3, Thompson, Morrison, and WSM6 at Oliktok from 1200 UTC on the 26th to 1200 UTC on the 27th. LWP from ERA5 is shown in black, dashed lines.

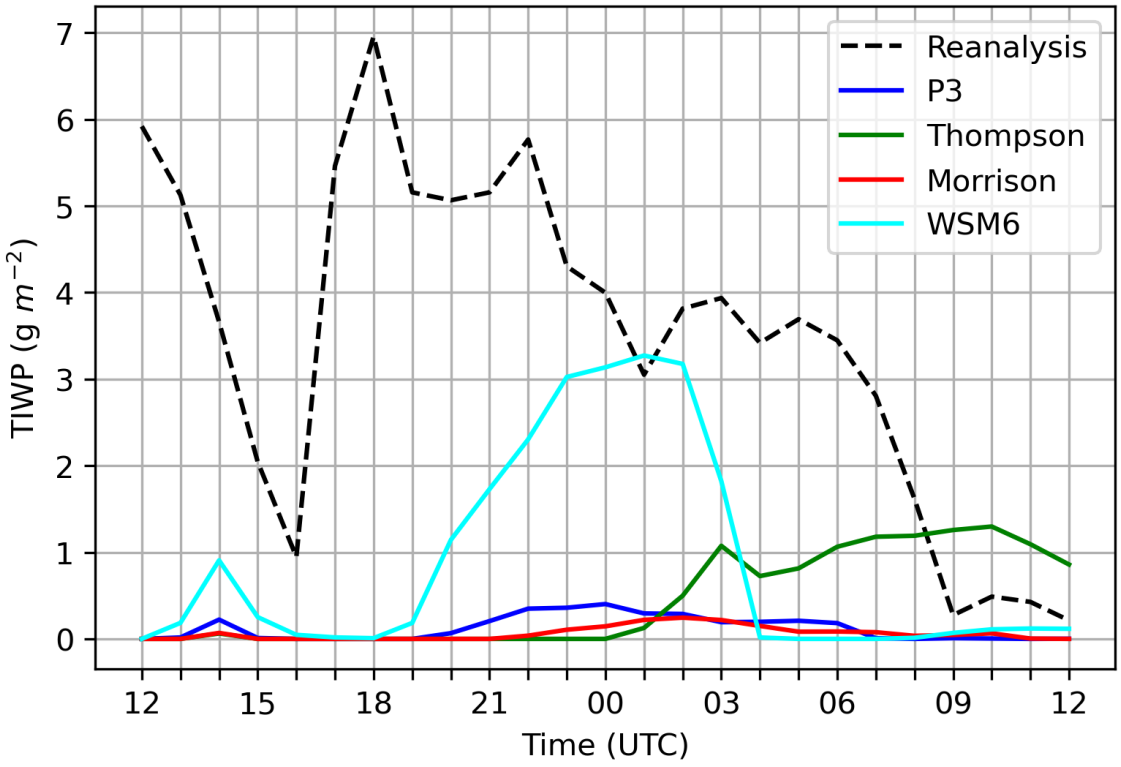

Figure 9. TIWP produced by P3, Thompson, Morrison, and WSM6 at Oliktok from 1200 UTC on the 26th to 1200 UTC on the 27th. TIWP from ERA5 is shown in black, dashed lines.

Thompson produced the largest quantities of snow mixing ratio, leading to SWP of up to 1.2 $g\,m^{-2}$. Production of snow in Thompson did not begin until around four hours after cloud formation, and was mostly evenly distributed throughout the cloud layer, extending down to the surface in the last several hours of the simulation.

4.1.3 Precipitation

Figure 10 shows total hourly precipitation rates from observation and as produced by each model. Maximum precipitation rates form observation were 0.04 $mm\,hr^{-1}$ near 0700 and 1000 UTC on the 27th. There were slight increases of up to 0.005 $mm\,hr^{-1}$ right around 0000 UTC on the 27th, and minimal precipitation throughout the rest of the time.

P3 produced a maximum total precipitation rate of up to 0.001 $mm\,hr^{-1}$, which occurred during the same time as the slight increases observed. P3 was not able to capture the larger rates of precipitation that occurred during the last few hours of the simulation. Thompson was not able to produce the increased rates of precipitation around 0000 UTC on the 27th but was able to produce 0.005 $mm\,hr^{-1}$ of precipitation during the last few hours of simulation. The values of precipitation rates from Thompson were about an order of magnitude lower than observed, but followed a reasonably similar trajectory, especially through the tail end of the simulation.

Morrison was unable to produce more than 0.0002 $mm\,hr^{-1}$ of total precipitation rate, but did however match the trend in the last few hours of simulation as compared to observation. WSM6 produced up to 0.005 $mm\,hr^{-1}$ of precipitation rate just shortly after 0000 UTC on the 27th, matching up well with the observation at the same time. The last few hours of simulation WSM6 produced up to 0.005 $mm\,hr^{-1}$ of precipitation, about one order of magnitude lower than observed, but matching the general trend of the observed values. The precipitation produced by WSM6 in

the first few hours of simulation climbed up to $\sim$0.008 $mm\,hr^{-1}$, however this was during the "spin up" time of the model run, and would be difficult to comment on why precipitation was generated at this time.

All of the precipitation produced by each model was entirely snow which is highlighted in Figure 11. P3 produced a maximum of $7 \times 10^{-4} mm\,hr^{-1}$ snow at around 2200 UTC in the simulation, with a secondary peak of $5 \times 10^{-4} mm\,hr^{-1}$ seven hours after that. Thompson began producing precipitation at the half-way point of simulation (0000 UTC), which increased to a maximum of $2 \times 10^{-3} mm\,hr^{-1}$ of snow by the end of the simulation. The precipitation pattern from Thompson matches more closely to the general trend of the observation than P3. Morrison produced even lower amounts of snow precipitation, peaking twice with values of $\sim 8 \times 10^{-5} mm\,hr^{-1}$ at 0500 UTC and 1000 UTC in the simulation. WSM6 produced a very small maximum $10^{-6} mm\,hr^{-1}$ of graupel at around three hours into the simulation. This value is extremely low, and as it occurred during just the first few hours of spin up, would be difficult to discern exactly why. Snow precipitation from WSM6 maximized just a few hours into the simulation at $4 \times 10^{-3} mm\,hr^{-1}$. Two subsequent peaks occurred at around 0200 UTC and 1000 UTC in the simulation of $2 \times 10^{-3} mm\,hr^{-1}$.

4.1.4 Vertical Profiles

P3, Morrison, and WSM6 all produced very similar vertical profiles as shown in figure 12. At 0000 UTC in the lowest 700 m, they each produce a warm bias of ~ 2 K. The base of the upper inversion from these schemes begins at around 550 m, and the magnitude of the inversion layer is much less than was observed as highlighted in figure 13. Peak inversion strength for these three models was 0.02 $K\,m^{-1}$, or about a factor of five less than observed. The patterns produced by these schemes relative to observation follow similarly at the 0600 UTC profile, with the exception

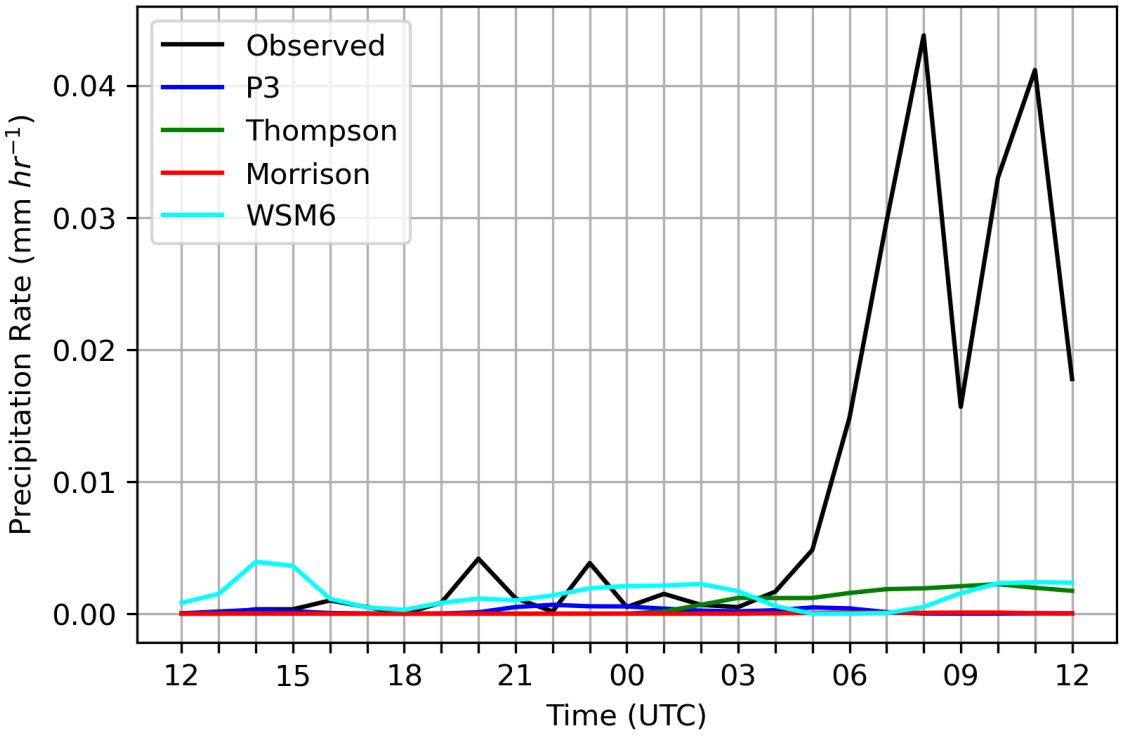

Figure 10. Total precipitation rate ($mm\,hr^{-1}$) observed and produced by P3, Thompson, Morrison, and WSM6 at Oliktok from 1200 UTC on the 26th to 1200 UTC on the 27th.

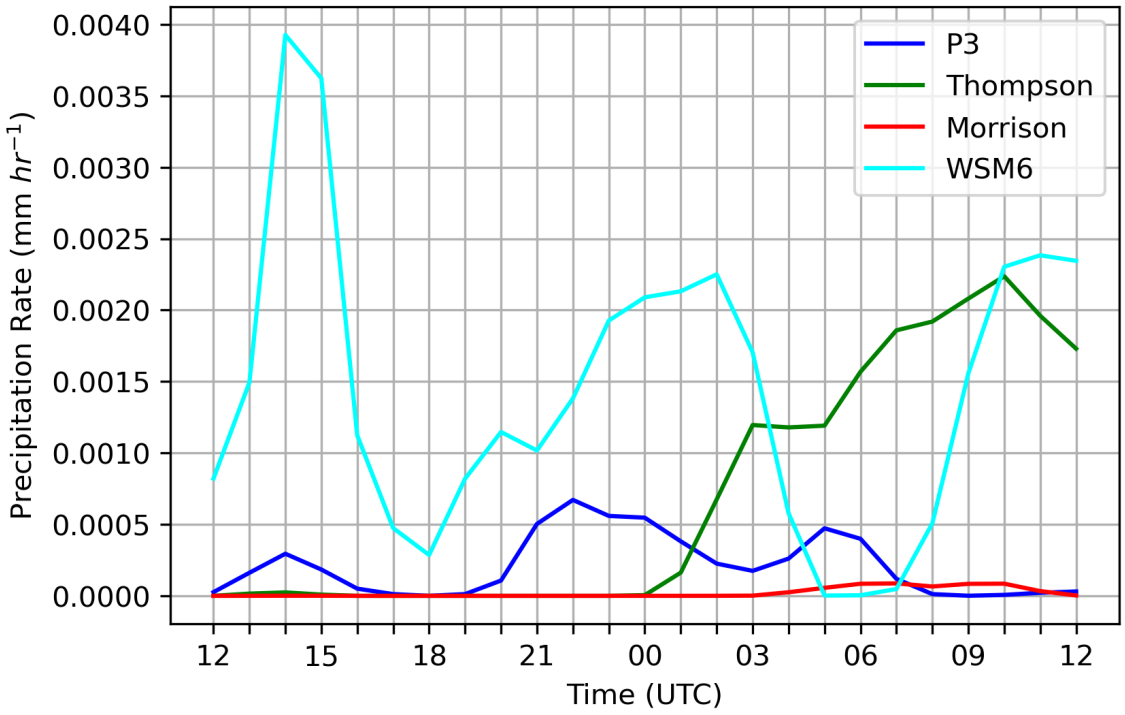

Figure 11. Snow precipitation ($mm\,hr^{-1}$) produced by P3, Thompson, Morrison, and WSM6 at Oliktok from 1200 UTC on the 26th to 1200 UTC on the 27th.

that each one produced a surface-based inversion in the lowest 50-100 m of up to 0.05 $K\,m^{-1}$. This surface-based inversion was likely due to the lower cloud top and optically thin, all ice (absent) cloud produced by P3 and Morrison (WSM6), which led to less longwave radiation being absorbed and re-emitted by the cloud layer down to the surface, resulting in lower surface temperatures.

Relative humidity from each of these models, shown in figure 14, was also underestimated at 0000 UTC by 3-4% in the lower boundary layer and as much as 20% near cloud top. One possible explanation for this is that each of these three models overestimated temperature and relative humidity just above cloud top from $\sim$ 750-1000 m, and drastically overestimated relative humidity from $\sim$ 1000-1500 m. There was no clear way to extract vertical velocities from observations because it is not possible to distinguish between larger falling precipitation particles and the smaller particles

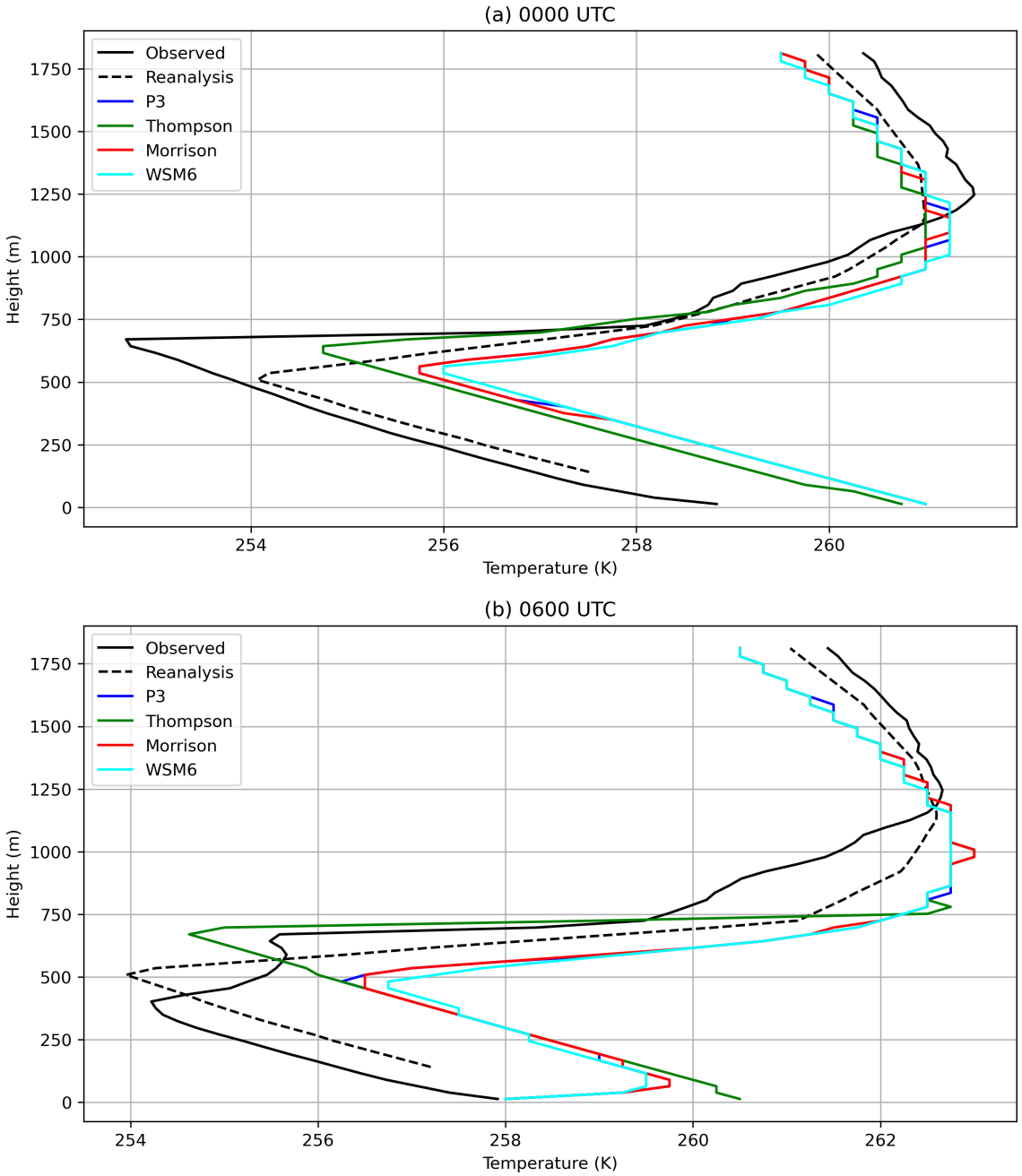

Figure 12. Temperature profile observed and produced by P3, Thompson, Morrison, and WSM6 for (a) 0000 UTC and (b) 0600 UTC on the 27th. Reanalysis temperature from ERA5 is also plotted for reference.

that follow the air motions, but subsidence above cloud top from P3, Morrison, and WSM6 were all less than 1 $cm\,s^{-1}$. This likely also stems from the lack of cloud top cooling and turbulent motions to help mix moisture into the boundary layer from above.

Thompson did not follow suit with the rest of the schemes on vertical temperature profile. It still produced a warm bias of $\sim 2\ K$ in the lowest $\sim 700\ m$ at 0000 UTC, but the inversion layer began higher up, within $\sim 50\ m$ of the observation. The magnitude of the elevated inversion is stronger with Thompson, peaking at $\sim 0.04\ K\,m^{-1}$, and also matches more closely to observation, although still slightly more than a factor of two smaller. The stronger inversion and heightened inversion base in Thompson are likely due to the presence of liquid water within the cloud layer generated, producing stronger radiative cooling near the cloud top. This cooling combined with a higher cloud top resulted in Thompson matching more closely with observations.

At 0600 UTC Thompson maintained its constant equivalent potential temperature down to the surface (not shown) and did not produce a surface-based inversion. This was likely due to the optically thicker cloud absorbing and re-emitting longwave radiation near the surface and additional cooling resulting in the continued coupling of Thompson's cloud layer and a well-mixed boundary layer down to the surface. Thompson did not capture the temperature profile at cloud top as well at 0600 UTC. The magnitude of the cloud top inversion at this time produced by Thompson was $0.14\ K\,m^{-1}$, or roughly a factor of two larger than observed. Turbulent motions near the cloud top in observations resulted in the mixing of warmer air from above and below, which Thompson was not able to resolve. This might be remedied by a higher vertical resolution in the boundary layer, but was not analyzed in this study. Relative humidity in Thompson matched up better with observations than the other three models, especially near cloud top, where values were within $\sim 10\%$ of observed at

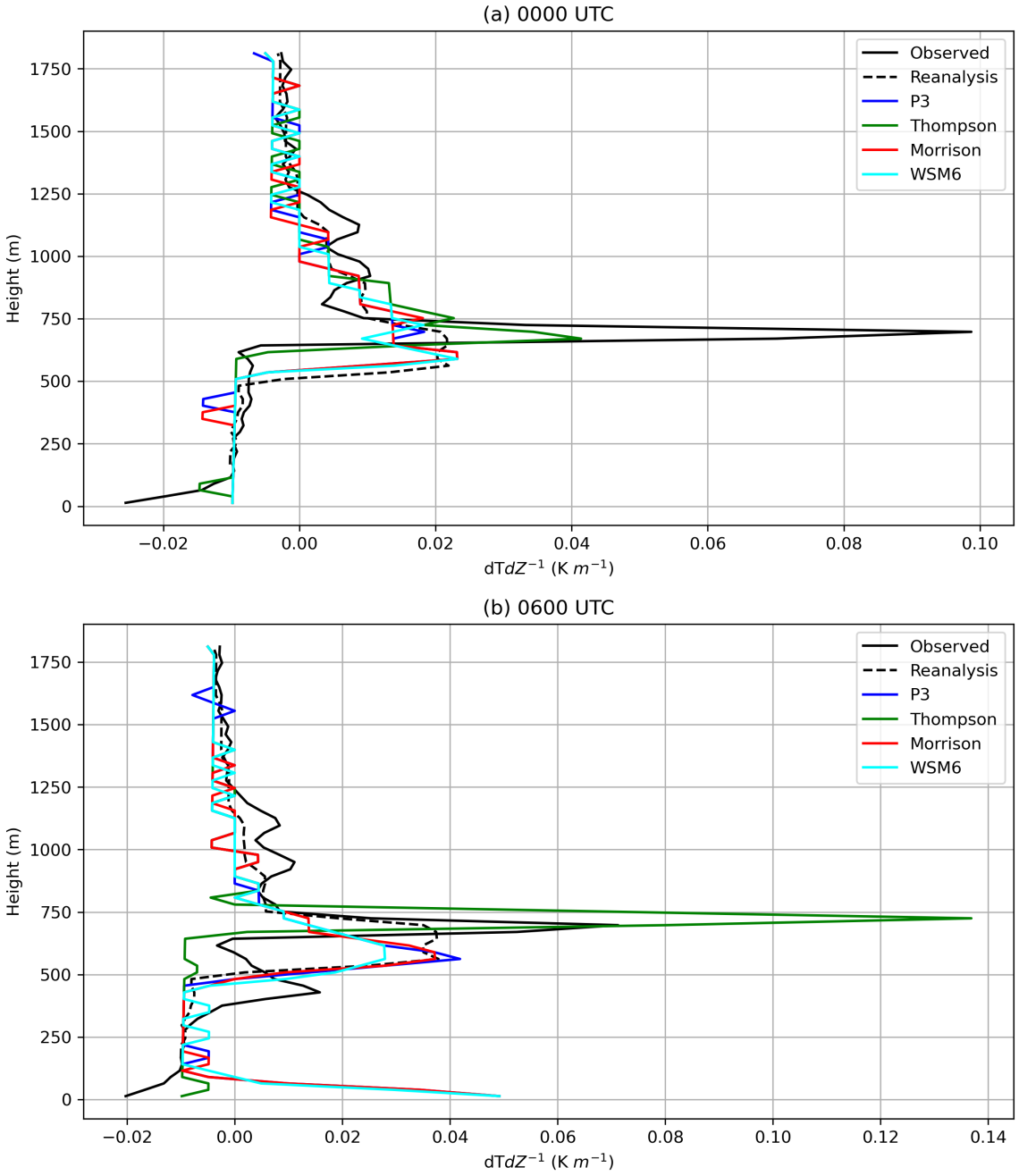

Figure 13. $\frac{\Delta T}{\Delta Z}$ **profile observed and produced by P3, Thompson, Morrison, and WSM6 for (a) 0000 UTC and (b) 0600 UTC on the 27th. Reanalysis temperature from ERA5 is also plotted for reference.**

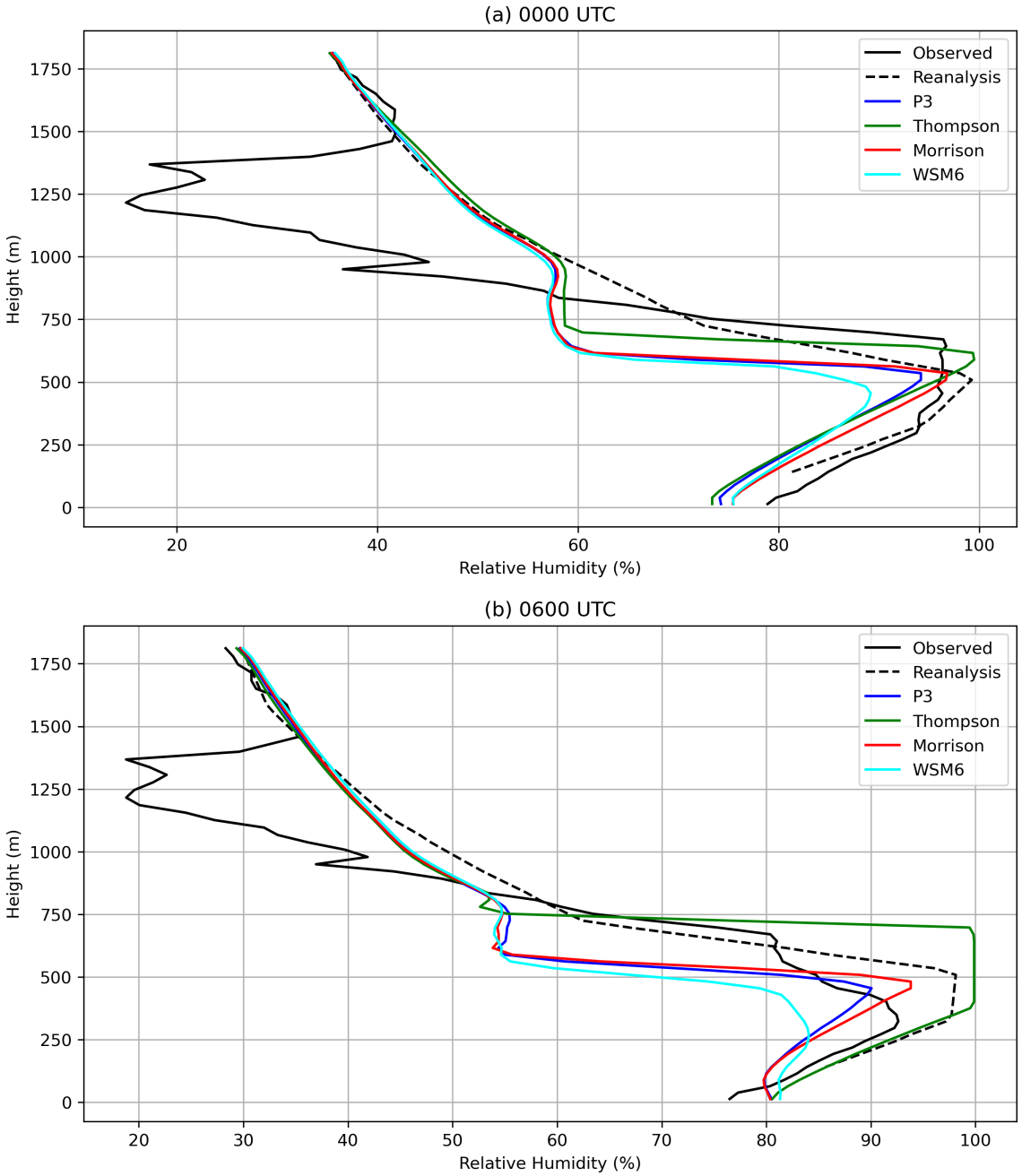

Figure 14. Relative humidity profile observed and produced by P3, Thompson, Morrison, and WSM6 for (a) 0000 UTC and (b) 0600 UTC on the 27th. Reanalysis temperature from ERA5 is also plotted for reference.

0000 UTC. At 0600 UTC, Thompson overestimated relative humidity values within the boundary layer by 10-15%, maximizing at cloud top. The overestimation in relative humidity at 0600 UTC by Thompson is likely due to lower temperatures near cloud top as a result of stronger radiative cooling, and less mixing from above cloud top compared to observation.

4.2 Discussion

4.2.1 Model Performance

It is likely that each microphysics scheme was not given the proper opportunity to simulate the AMPS case in this study. The ERA5 dataset was chosen to initialize each simulation as it was shown to perform relatively well over the Arctic region (Graham et al., 2019) compared to similar reanalysis datasets. However, due to the lack of ground-based observational data at high latitudes, it is not possible to verify the accuracy of the ERA5 over much of the spatial extent of the domains used here (conditions from ERA5 not shown unless referenced otherwise). The warm bias in in the boundary layer from ERA5 (shown in figure 12) is not enough to account for the warm biases of each simulation. ERA5 struggled to account for much of the low-level cloud cover upstream (back trajectory of winds) within domain one and in many areas surrounding Oliktok. There were relatively low values of cloud liquid water in ERA5 in the areas surrounding Oliktok early in the simulation time frame and relatively lower values (compared to Oliktok) of water vapor mixing ratio upstream of Oliktok.

Since each model run relies so heavily on the initial boundary conditions, it is possible that the physical conditions (temperature, specific humidity, cloud liquid, etc.) from ERA5, which ultimately were advected into the nested domains, were biased to be warmer and slightly drier than the real-world conditions. This would lead to issues in relative humidity (and supersaturation) values within the boundary

layer at Oliktok, inhibiting condensation from each of the microphysics schemes. The lack of cloud liquid water and larger fraction of ice within the clouds upstream of Oliktok could mean that much of the boundary layer became decoupled within the model due to lack of absorption and re-emission of longwave radiation, which would inhibit surface level moisture from entering the cloud layers. It is still unclear exactly why each of the simulations became so warm so quickly ($\sim 2\ K$ within six hours), but the magnitude to which any biases in ERA5 influence the deviation in each simulation from observation will be the subject of research and is not further analyzed here.

4.2.2 WSM6

WSM6 resulted in the cloud pattern and properties least similar to observations. The cloud produced was short-lived, and entirely made up of ice particles. Precipitation of ice early on from WSM6 likely aided the fate of the cloud layer through removal of moisture in the boundary layer. Additionally, WSM6 calculates ice nucleation rates and, subsequently, auto conversion rates from liquid to ice based on temperature. WSM6 also assumed that ice nuclei number concentration is a function of temperature, and that ice number concentration is a function of ice amount. The main process for ice generation in WSM6 was likely due to over-active deposition. The quick and biased ice production in WSM6 and early snowfall likely led to the rapid formation and dissipation of the cloud layer. Table 3 shows the average real-world time to compute each timestep within the model. WSM6 was the fastest scheme and completed the simulation $\sim 8\%$ faster than the slowest scheme, Morrison.

4.2.3 P3 and Morrison

P3 took $\sim 4\%$ less time to run than Morrison, but both similarly produced all-ice clouds, which formed around 2000 UTC and dissipated almost completely by the

Table 3. Real-world average time (s) to compute each time step of the model for each microphysics scheme and domain.

	Domain 1	Domain 2	Domain 3	Domain 4
P3	7.6422	3.3724	1.1334	0.1949
Thompson	7.8683	3.4951	1.1830	0.2073
Morrison	7.9920	3.5405	1.2080	0.2097
WSM6	7.4261	3.2771	1.1123	0.1964

end of the simulation. No significant liquid water was produced by either scheme throughout the duration of the simulation, which likely resulted in the fate of the clouds produced. Lack of liquid water production in both of these schemes is likely due to the way they treat CCN and INPs. P3 and Morrison contained a large number of aerosols initially and allows them to act as INP, which resulted in early and frequent development of ice particles. The main issue here is not that P3 and Morrison could not produce liquid based on the dynamical conditions, but rather were biased toward ice production. Once ice is over-produced within these clouds, glaciation can quickly take effect, and any liquid water which forms is quickly converted to ice before it can exist very long.

There is evidence of this as both P3 and Morrison produced a very small amount of liquid water shortly after cloud formation, which quickly dissipated, leaving only ice particles to remain. There is also the possibility that P3 and Morrison generated liquid water at certain time steps within the simulation, but contact and immersion freezing may have quickly turned those particles into ice. Additionally, subgrid-scale vertical velocity for droplet activation is not used in these schemes so any vertical motions that are not explicitly resolved by the simulation cannot drive droplet activation. This limitation along with the relatively "low" resolution of the boundary layer, and above cloud top, likely inhibited droplet activation.

4.2.4 Thompson

Thompson performed the best relative to the other three models in representing the cloud pattern and properties as compared with observations and was the second slowest scheme for calculations, running just 2% faster than Morrison. Thompson's cloud formed at $\sim$ 0000 UTC, and persisted through the rest of the simulation. Thompson's cloud was sustained by the production of supercooled liquid water, which aided cloud top radiative cooling and the continued coupling with the surface, allowing moisture transport from within the boundary layer into the cloud layer.

The process by which Thompson produced liquid water is slightly different than the rest of the schemes as Thompson used an initial aerosol concentration which was one or two orders of magnitude smaller than P3 and Morrison, and treats those aerosols as "liquid friendly" or "ice friendly". The reason Thompson produced more liquid water is likely both microphysical and not. The lack of ice production did not result in quick glaciation of the cloud layer as it may have in P3 and Morrison, which allowed supercooled liquid droplet activation through subsequent iterations. P3 and Morrison likely produced more numerous, smaller-sized ice particles, which resulted in a larger total surface area available for deposition freezing, and further ice growth, while Thompson likely produced a smaller number of larger-sized ice particles. Additionally, the advection of "liquid friendly" and "ice friendly" aerosols within the domain likely resulted in a continuous supply of available nucleation particles, allowing both ice and liquid to exist. It's likely that collisions between ice and cloud liquid occurred within Thompson, however the resultant riming did not reach the threshold for conversion to graupel from snow. Minimal turbulent motions within Thompson and lack of collisions between species may also be a reason that both liquid and ice persisted, although further research is needed to confirm this.

V. Conclusion

5.1 Summary and Conclusions

AMPS clouds are an important aspect of the Arctic-climate system and strongly affect the surface radiation budget over the Arctic throughout the year. The misrepresentation of AMPS clouds within operational and climate models can have significant impacts on surface temperatures and boundary layer conditions, which can result in a feedback of further errors. Studying the microphysical properties of AMPS will aid their accurate simulation and reduce the error and uncertainty in future studies.

In this study, four LES simulations were conducted using four different microphysics schemes in WRF-ARW. The P3, Thompson, Morrison, and WSM6 schemes were used to simulate the cloud pattern and properties of an AMPS cloud which occurred on 26 and 27 April, 2017 near Oliktok Point, AK. The WSM6 scheme produced the shortest-lived cloud, which was made up entirely of cloud ice. This gave rise to errors in surface-based inversion values, as well as the temperature profile throughout the rest of the simulation. While single-moment schemes can be advantageous as they generally are cheaper on computational resources, they perhaps lack the sophistication of double-moment schemes by an oversimplified PSD.

P3 and Morrison both produced clouds, which matched the general shape of the observations, but both consisted of almost entirely ice. Very little liquid water was present in the clouds produced by these two models, which was likely a result of a large number of INPs and overactive ice nucleation rates. The consequences from both of these models were the dissipation of the cloud layer and deviations in temperature profiles from observation.

Thompson performed the best of all four schemes and, in fact, was the only model to produce a significant mixed-phased cloud, although it still lacked accuracy

compared with observation. LWP values from Thompson reached up to around 50 $g\,m^{-2}$ toward the end of the simulation, which lined up well with observations. Although rimed particles were not produced by Thompson (or any of the microphysics schemes), the supercooled liquid water aided in the cloud top radiative cooling, which likely helped drive vertical motions and moisture into the cloud layer from the surface. This, coupled with smaller a number of INPs and adequate a number of CCN allowed for the persistence of Thompson's cloud layer. Because liquid water existed and created an optically thick cloud in Thompson, a surface-based inversion did not form at 0600 UTC as it did with the other three schemes, which resulted in Thompson matching up more closely with observations.

The better performance of Thompson, P3, and Morrison is an indication that PSD representation through double-moment schemes is likely an important factor in the accurate simulation of AMPS. The cloud particle species generated in Thompson are an indication that the treatment of aerosols to act as INP or CCN is also very important to properly capture the cloud pattern and properties of AMPS.

5.2 Recommendations for Future Research

Future research on simulating AMPS at LES scales should include a thorough investigation on the impact of aerosol concentration to act as INP or CCN within the model. This would consist of picking one or two of the microphysics schemes used and performing a sensitivity test, varying aerosol concentration and/or INP and CCN to identify the different structure and properties in the clouds simulated. Aerosol concentrations should be altered within the microphysics scheme code to reflect the amount observed either climatologically or by direct observation. This also implies the analysis of different cases of persistent AMPS within the Arctic region, possibly at locations other than Oliktok as well.

Boundary conditions, horizontal and vertical resolutions, and domain size should also be further examined. Future studies should explore the possibility of different surface parameterizations or forcing data which can, in some form, account for possible leads in sea ice or other sources of heat and moisture which can affect AMPS development. Increasing resolution may also help to better resolve vertical motions in the boundary layer, which can aid nucleation based on vertical velocities in P3, Thompson, and Morrison.

Finally, one scheme should be chosen to perform an idealized simulation of AMPS. This should include the use of WRF's nudging capability, to recreate the cloud pattern and properties artificially, and study the impacts to the microphysical process. This will provide insight on the microphysics involved in AMPS, and possibly provide the opportunity to better parameterize the complex nature of high-latitude mixed-phase clouds.

References

ARM Climate Research Facility. (2013a). *Balloon-Borne Sounding System (SONDEWNPN).* 2016-08-22 to 2018-09-01, ARM Mobile Facility (OLI) Oliktok Point, Alaska; AMF3 (M1). Compiled by Compiled by D. Holdridge, J. Kyrouac and R. Coulter. ARM Data Center: Oak Ridge, Tennessee, USA. Data set accessed 2018-11-19 at http://dx.doi.org/10.5439/1021460.

ARM Climate Research Facility. (2013b). *Interpolated Sonde (INTERPOLATEDSONDE).* 2017-04-24 to 2017-04-30, ARM Mobile Facility (OLI) Oliktok Point, Alaska; AMF3 (M1). Compiled by S. Giangrande and T. Toto. ARM Data Center: Oak Ridge, Tennessee, USA. Data set accessed 2018-12-15 at http://dx.doi.org/10.5439/1095316.

ARM Climate Research Facility. (2013c). *Surface Meteorological Instrumentation (MET).* 2014-11-11 to 2018-09-09, ARM Mobile Facility (OLI) Oliktok Point, Alaska; AMF3 (M1). Compiled by M. Ritsche, J. Kyrouac, N. Hickmon and D. Holdridge. ARM Data Center: Oak Ridge, Tennessee, USA. Data set accessed 2019-10-09 at http://dx.doi.org/10.5439/1025220.

ARM Climate Research Facility. (2014). *Multi-Angle Snowflake Camera (MASC).* 2015-11-29 to 2018-08-31, ARM Mobile Facility (OLI) Oliktok Point, Alaska; AMF3 (M1). Compiled by B. Ermold, K. Shkurko, and M. Stuefer. ARM Data Center: Oak Ridge, Tennessee, USA. Data set accessed 2019-08-11 at http://dx.doi.org/10.5439/1234550.

ARM Climate Research Facility. (2015). *Active Remote Sensing of CLouds (ARSCL) product using Ka-band ARM Zenith Radars (ARSCLKAZR1KOLLIAS).* 2015-11-29 to 2018-09-10, ARM Mobile Facility (OLI) Oliktok Point, Alaska; AMF3 (M1). Compiled by Compiled by K. Johnson, T. Toto and S. Giangrande. ARM Data Center: Oak Ridge, Tennessee, USA. Data set accessed 2019-10-14 at http://dx.doi.org/10.5439/1350629.

Bulatovic, I., Igel, A. L., Leck, C., Heintzenberg, J., Riipinen, I., & Ekman, A. M. (2021, 3). The importance of Aitken mode aerosol particles for cloud sustenance in the summertime high Arctic-A simulation study supported by observational data. *Atmospheric Chemistry and Physics*, *21*, 3871-3897. doi: 10.5194/acp-21-3871-2021

Cadeddu, M. (2021). *Microwave Radiometer-3-Channel (MWR3C) Instrument Handbook MP Cadeddu.*

Cadeddu, M. P., Liljegren, J. C., & Turner, D. D. (2013). The atmospheric radiation measurement (ARM) program network of microwave radiometers: Instrumentation, data, and retrievals. *Atmospheric Measurement Techniques*, *6*, 2359-2372. doi: 10.5194/amt-6-2359-2013

Chiacchio, M., Francis, J., & Stackhouse, P. (2002). Evaluation of methods to estimate the surface downwelling longwave flux during Arctic winter. , *41*, 306–318.

Clothiaux, E. E., Ackerman, T. P., Mace, G. G., Moran, K. P., Marchand, R. T., Miller, M. A., ... Martner, B. E. (2000). *Objective Determination of Cloud Heights and Radar Reflectivities Using a Combination of Active Remote Sensors at the ARM CART Sites.*

Collins, W. D., Rasch, P. J., Boville, B. A., Hack, J. J., Mccaa, J. R., Williamson, D. L., ... Dai, Y. (2004). *Description of the NCAR Community Atmosphere Model (CAM 3.0).*

Computational and Information Systems Laboratory. (2019).

Curry, J., Rossow, W., Randall, D., & Schramm, J. (1996). Overview of Arctic Cloud and Radiation Characteristics. *Journal of Climate*, *9*, 1731-1764. doi: https://doi.org/10.1175/1520-0442(1996)009%3C1731:OOACAR%3E2.0.CO;2

Dodson, J. B., Taylor, P., Moore, R., Bromwich, D., Hines, K., Thornhill, K., ... Bennett, J. (2020). Evaluation of Simulated Cloud Water in Low Clouds over the Beaufort Sea in Arctic System Reanalysis using ARISE Airborne In Situ Observations. *Atmospheric Chemistry and Physics*, 1-26. doi: 10.5194/acp-2020-1003

Fitch, K. E., & Garrett, T. J. (2022). Graupel Precipitating From Thin Arctic Clouds With Liquid Water Paths Less Than 50 g m- 2. *Geophysical Research Letters*, *49*(1), e2021GL094075. doi: https://doi.org/10.1029/2021GL094075

Fridlind, A. M., Ackerman, A. S., McFarquhar, G., Zhang, G., Poellot, M. R., DeMott, P. J., ... Heymsfield, A. J. (2007, 12). Ice properties of single-layer stratocumulus during the Mixed-Phase Arctic Cloud Experiment: 2. Model results. *Journal of Geophysical Research Atmospheres*, *112*. doi: 10.1029/2007JD008646

Garrett, T. J., Fallgatter, C., Shkurko, K., & Howlett, D. (2012). Fall speed measurement and high-resolution multi-angle photography of hydrometeors in free fall. *Atmospheric Measurement Techniques*, *5*, 2625-2633. doi: 10.5194/amt-5-2625-2012

Garrett, T. J., & Yuter, S. E. (2014, 9). Observed influence of riming, temperature, and turbulence on the fallspeed of solid precipitation. *Geophysical Research Letters*, *41*, 6515-6522. doi: 10.1002/2014GL061016

Garrett, T. J., Yuter, S. E., Fallgatter, C., Shkurko, K., Rhodes, S. R., & Endries, J. L. (2015, 6). Orientations and aspect ratios of falling snow. *Geophysical Research Letters*, *42*, 4617-4622. doi: 10.1002/2015GL064040

Graham, R. M., Cohen, L., Ritzhaupt, N., Segger, B., Graversen, R. G., Rinke, A., ... Hudson, S. R. (2019). Evaluation of six atmospheric reanalyses over Arctic sea ice from winter to early summer. *Journal of Climate*, *32*, 4121-4143. doi: 10.1175/JCLI-D-18-0643.1

Griesche, H. J., Ohneiser, K., Seifert, P., Radenz, M., Engelmann, R., & Ansmann, A. (2021, 7). Contrasting ice formation in Arctic clouds: Surface-coupled vs. surface-decoupled clouds. *Atmospheric Chemistry and Physics*, *21*, 10357-10374. doi: 10.5194/acp-21-10357-2021

Hersbach, H., Bell, B., Berrisford, P., Hirahara, S., Horányi, A., Muñoz-Sabater, J., ... Thépaut, J. N. (2020, 7). The ERA5 global reanalysis. *Quarterly Journal of the Royal Meteorological Society*, *146*, 1999-2049. doi: 10.1002/qj.3803

Hong, S.-Y., Noh, Y., & Dudhia, J. (2006). *A New Vertical Diffusion Package with an Explicit Treatment of Entrainment Processes.*

Intrieri, J. M., Shupe, M. D., Uttal, T., & McCarty, B. J. (2002, 10). An annual cycle of Arctic cloud characteristics observed by radar and lidar at SHEBA. *Journal of Geophysical Research: Oceans*, *107*. doi: 10.1029/2000jc000423

Jiménez, P. A., Dudhia, J., González-Rouco, J. F., Navarro, J., Montávez, J. P., & García-Bustamante, E. (2012, 3). A revised scheme for the WRF surface layer formulation. *Monthly Weather Review*, *140*, 898-918. doi: 10.1175/MWR-D-11-00056.1

Kirpes, R. M., Bonanno, D., May, N. W., Fraund, M., Barget, A. J., Moffet, R. C., ... Pratt, K. A. (2019, 11). Wintertime Arctic Sea Spray Aerosol Composition Controlled by Sea Ice Lead Microbiology. *ACS Central Science*, *5*, 1760-1767. doi: 10.1021/acscentsci.9b00541

Li, X., Krueger, S. K., Strong, C., Mace, G. G., & Benson, S. (2020, 12). Midwinter Arctic leads form and dissipate low clouds. *Nature Communications*, *11*. doi: 10.1038/s41467-019-14074-5

Maahn, M., Goren, T., Shupe, M. D., & de Boer, G. (2021, 9). Liquid Containing Clouds at the North Slope of Alaska Demonstrate Sensitivity to Local Industrial Aerosol Emissions. *Geophysical Research Letters*, *48*. doi: 10.1029/2021GL094307

Milbrandt, J. A., & Yau, M. K. (2005). *A Multimoment Bulk Microphysics Parameterization. Part II: A Proposed Three-Moment Closure and Scheme Description.*

Morris, V. R. (2016). *Ceilometer Instrument Handbook.*

Morrison, A. L., Kay, J. E., Frey, W. R., Chepfer, H., & Guzman, R. (2019, 1). Cloud Response to Arctic Sea Ice Loss and Implications for Future Feedback in the CESM1 Climate Model. *Journal of Geophysical Research: Atmospheres*, *124*, 1003-1020. doi: 10.1029/2018JD029142

Morrison, H., Boer, G. D., Feingold, G., Harrington, J., Shupe, M. D., & Sulia, K. (2012, 1). Resilience of persistent Arctic mixed-phase clouds. *Nature Geoscience*, *5*, 11-17. doi: 10.1038/ngeo1332

Morrison, H., & Milbrandt, J. A. (2015). Parameterization of cloud microphysics based on the prediction of bulk ice particle properties. Part I: Scheme description and idealized tests. *Journal of the Atmospheric Sciences*, *72*. doi: 10.1175/JAS-D-14-0065.1

Morrison, H., Thompson, G., & Tatarskii, V. (2009). Impact of cloud microphysics on the development of trailing stratiform precipitation in a simulated squall line: Comparison of one- and two-moment schemes. *Monthly Weather Review*, *137*. doi: 10.1175/2008MWR2556.1

Murray, B. J., O'sullivan, D., Atkinson, J. D., & Webb, M. E. (2012, 9). Ice

nucleation by particles immersed in supercooled cloud droplets. *Chemical Society Reviews*, *41*, 6519-6554. doi: 10.1039/c2cs35200a

Neggers, R. A., Chylik, J., Egerer, U., Griesche, H., Schemann, V., Seifert, P., ... Macke, A. (2019). Local and Remote Controls on Arctic Mixed-Layer Evolution. *Journal of Advances in Modeling Earth Systems*, *11*, 2214-2237. doi: 10.1029/2019MS001671

Oue, M., Kumjian, M. R., Lu, Y., Jiang, Z., Clothiaux, E. E., Verlinde, J., & Aydin, K. (2015). X-band polarimetric and Ka-band Doppler spectral radar observations of a graupel-producing arctic mixed-phase cloud. *Journal of Applied Meteorology and Climatology*, *54*, 1335-1351. doi: 10.1175/JAMC-D-14-0315.1

Ovchinnikov, M., Ackerman, A. S., Avramov, A., Cheng, A., Fan, J., Fridlind, A. M., ... Sulia, K. (2014, 3). Intercomparison of large-eddy simulations of Arctic mixed-phase clouds: Importance of ice size distribution assumptions. *Journal of Advances in Modeling Earth Systems*, *6*, 223-248. doi: 10.1002/2013MS000282

Quinn, P. K., Miller, T. L., Bates, T. S., Ogren, J. A., Andrews, E., & Shaw, G. E. (2002, 6). A 3-year record of simultaneously measured aerosol chemical and optical properties at Barrow, Alaska. *Journal of Geophysical Research: Atmospheres*, *107*. doi: 10.1029/2001jd001248

Report to Congress Department of Defense Arctic Strategy. (2019). Retrieved from `https://media.defense.gov/2019/Jun/06/2002141657/-1/-1/1/2019-DOD-ARCTIC-STRATEGY.PDF`

Sedlar, J., Igel, A., & Telg, H. (2021, 3). Processes contributing to cloud dissipation and formation events on the North Slope of Alaska. *Atmospheric Chemistry and Physics*, *21*, 4149-4167. doi: 10.5194/acp-21-4149-2021

Shupe, M. D., Kollias, P., Persson, P. O. G., & McFarquhar, G. M. (2008, 4). Vertical motions in arctic mixed-phase stratiform clouds. *Journal of the Atmospheric Sciences*, *65*, 1304-1322. doi: 10.1175/2007JAS2479.1

Silber, I., Fridlind, A. M., Verlinde, J., Ackerman, A. S., Cesana, G. V., & Knopf, D. A. (2021, 3). The prevalence of precipitation from polar supercooled clouds. *Atmospheric Chemistry and Physics*, *21*, 3949-3971. doi: 10.5194/acp-21-3949-2021

Skamarock, W. C., Klemp, J. B., Dudhia, J., Gill, D. O., Liu, Z., Berner, J., ... Huang, X.-Y. (2021). *A Description of the Advanced Research WRF Model Version 4.* Retrieved from `http://library.ucar.edu/research/publish-technote`

Solomon, A., Boer, G. D., Creamean, J. M., McComiskey, A., Shupe, M. D., Maahn, M., & Cox, C. (2018, 12). The relative impact of cloud condensation nuclei and ice nucleating particle concentrations on phase partitioning in Arctic mixed-phase stratocumulus clouds. *Atmospheric Chemistry and Physics*, *18*, 17047-17059. doi: 10.5194/acp-18-17047-2018

Solomon, A., Shupe, M. D., Persson, O., Morrison, H., Yamaguchi, T., Caldwell,

P. M., & Boer, G. D. (2014, 2). The sensitivity of springtime arctic mixed-phase stratocumulus clouds to surface-layer and cloud-top inversion-layer moisture sources. *Journal of the Atmospheric Sciences*, *71*, 574-595. doi: 10.1175/JAS-D-13-0179.1

Solomon, A., Shupe, M. D., Persson, P. O., & Morrison, H. (2011). Moisture and dynamical interactions maintaining decoupled Arctic mixed-phase stratocumulus in the presence of a humidity inversion. *Atmospheric Chemistry and Physics*, *11*, 10127-10148. doi: 10.5194/acp-11-10127-2011

Tewari, M., Chen, F., Wang, W., Dudhia, J., LeMone, M. A., Mitchell, K., ... Cuenca, R. (2004). noah. *20th conference on weather analysis and forecasting/16th conference on numerical weather prediction*, 11-15.

Thompson, G., & Eidhammer, T. (2014). A study of aerosol impacts on clouds and precipitation development in a large winter cyclone. *Journal of the Atmospheric Sciences*, *71*, 3636-3658. doi: 10.1175/JAS-D-13-0305.1

Thompson, G., Field, P. R., Rasmussen, R. M., & Hall, W. D. (2008). Explicit forecasts of winter precipitation using an improved bulk microphysics scheme. Part II: Implementation of a new snow parameterization. *Monthly Weather Review*, *136*. doi: 10.1175/2008MWR2387.1

Verlinde, J., Harrington, J. Y., McFarquhar, G. M., Yannuzzi, V. T., Avramov, A., Greenberg, S., ... Schofield, R. (2007, 2). The mixed-phase arctic cloud experiment. *Bulletin of the American Meteorological Society*, *88*, 205-221. doi: 10.1175/BAMS-88-2-205

Walsh, J. E., Kattsov, V. M., Chapman, W. L., Govorkova, V., & Pavlova, T. (2002). *Comparison of Arctic Climate Simulations by Uncoupled and Coupled Global Models.* Retrieved from `http://www.iarc.uaf.edu/acia.html` doi: https://doi.org/10.1175/1520-0442(2002)015\%3C1429:COACSB\%3E2.0.CO;2

Wang, D., Guo, J., Chen, A., Bian, L., Ding, M., Liu, L., ... Han, Y. (2020, 7). Temperature Inversion and Clouds Over the Arctic Ocean Observed by the 5th Chinese National Arctic Research Expedition. *Journal of Geophysical Research: Atmospheres*, *125*. doi: 10.1029/2019JD032136

Wang, X., & Key, J. R. (2005, 7). Arctic surface, cloud, and radiation properties based on the AVHRR polar pathfinder dataset. Part II: Recent trends. *Journal of Climate*, *18*, 2575-2593. doi: 10.1175/JCLI3439.1

Wendisch, M., MacKe, A., Ehrlich, A., LüPkes, C., Mech, M., Chechin, D., ... Zeppenfeld, S. (2019, 5). The Arctic Cloud Puzzle Using ACLOUD/PASCAL Multiplatform Observations to Unravel the Role of Clouds and Aerosol Particles in Arctic Amplification. *Bulletin of the American Meteorological Society*, *100*, 841-871. doi: 10.1175/BAMS-D-18-0072.1

Williams, K. W. (2004). *A Summary of Unmanned Aircraft Accident/Incident Data: Human Factors Implications.* Retrieved from `http://www.dtic.mil/cgi-bin/GetTRDoc?AD=ADA460102`

Yang, F., Ovchinnikov, M., & Shaw, R. A. (2013, 7). Minimalist model of ice

microphysics in mixed-phase stratiform clouds. *Geophysical Research Letters*, *40*, 3756-3760. doi: 10.1002/grl.50700

Yin, L., Ping, F., & Mao, J. (2017, 5). A comparative study between bulk and bin microphysical schemes of a simulated squall line in East China. *Atmospheric Science Letters*, *18*, 195-206. doi: 10.1002/asl.742

Zhao, X., Liu, X., Burrows, S. M., & Shi, Y. (2021, 2). Effects of marine organic aerosols as sources of immersion-mode ice-nucleating particles on high-latitude mixed-phase clouds. *Atmospheric Chemistry and Physics*, *21*, 2305-2327. doi: 10.5194/acp-21-2305-2021

REPORT DOCUMENTATION PAGE

Form Approved
OMB No. 0704–0188

1. REPORT DATE *(DD–MM–YYYY)*	2. REPORT TYPE	3. DATES COVERED *(From — To)*
24–03–2022	Master's Thesis	Sept 2020 — Mar 2022

4. TITLE AND SUBTITLE

Intercomparison of Four Microphysics Schemes in Simulating Persistent Arctic Mixed-Phase Stratocumulus Clouds

5a. CONTRACT NUMBER

5b. GRANT NUMBER

5c. PROGRAM ELEMENT NUMBER

6. AUTHOR(S)

Cleveland, Zachary A. Captain, U.S. Air Force

5d. PROJECT NUMBER

22P105

5e. TASK NUMBER

5f. WORK UNIT NUMBER

7. PERFORMING ORGANIZATION NAME(S) AND ADDRESS(ES)

Air Force Institute of Technology
Graduate School of Engineering and Management (AFIT/EN)
2950 Hobson Way
WPAFB OH 45433-7765

8. PERFORMING ORGANIZATION REPORT NUMBER

AFIT-ENP-MS-22-M-084

9. SPONSORING / MONITORING AGENCY NAME(S) AND ADDRESS(ES)

AFLCMC, Weather Branch
Lt Col Jack Evans
2240 B St (Bldg 11)
WPAFB OH 45433
DSN 785-2208, COMM 937-255-2208

ACC, Weather Requirements Branch
Maj Kerrin Caldwell
204 Dodd Blvd Ste 311 (Bldg 602)
JB Langley-Eustis VA 23665
DSN 574-6330, COMM 757-764-6330

10. SPONSOR/MONITOR'S ACRONYM(S)

AFLCMC/XAW; ACC A5/8/9/A5W

11. SPONSOR/MONITOR'S REPORT NUMBER(S)

12. DISTRIBUTION / AVAILABILITY STATEMENT

DISTRIBUTION STATEMENT A:
APPROVED FOR PUBLIC RELEASE; DISTRIBUTION UNLIMITED.

13. SUPPLEMENTARY NOTES

14. ABSTRACT

A Large Eddy Simulation of a case study of a persistent AMPS cloud was conducted using the WRF-ARW model. The produced cloud pattern and properties of four different microphysics schemes – P3, Thompson, Morrison, and WSM6 – are compared to observations. Results show that the Thompson scheme was able to best simulate observed conditions as a result of fewer aerosols acting as ice nucleating particles, which allowed the production of more liquid water within the cloud layer. Thompson was the only parameterization scheme to produce significant cloud liquid water, which resulted in additional cloud top radiative cooling, continued coupling with the surface, and sustainment of the cloud layer. The lack of cloud liquid water produced in the other three schemes resulted in the early dissipation of their cloud layers and, consequently, stronger surface cooling, which led to production of a surface-based inversion and a decoupling of the cloud layer. Due to the Thompson scheme's more accurate representation of the cloud structure, it also captured surface and cloud top temperatures which aligned more closely to observations.

15. SUBJECT TERMS

Meteorology, Arctic, Weather, Clouds, Microphysics

16. SECURITY CLASSIFICATION OF:			17. LIMITATION OF ABSTRACT	18. NUMBER OF PAGES	19a. NAME OF RESPONSIBLE PERSON
a. REPORT	b. ABSTRACT	c. THIS PAGE			Lt Col Kyle E. Fitch, Ph.D, AFIT/ENP
U	U	U	U	59	19b. TELEPHONE NUMBER *(include area code)* (937) 255-3636, x4518; kyle.fitch@afit.edu